FINITE ELEMENT INVESTIGATION OF PRE-DAMAGED RC COLUMNS RETROFITTED WITH FRCM

by

Muhammad Kyaure

A Thesis presented to the Faculty of the
American University of Sharjah
College of Engineering
In Partial Fulfillment
of the Requirements
for the Degree of

Master of Science in

Civil Engineering

Sharjah, United Arab Emirates

June 2021

Declaration of Authorship

I declare that this thesis is my own work and, to the best of my knowledge and belief, it does not contain material published or written by a third party, except where permission has been obtained and/or appropriately cited through full and accurate referencing.

Signed: Muhammad Kyaure

Date: 30/06/2021

Approval Signatures

We, the undersigned, approve the Master's Thesis of Muhammad Kyaure

Thesis Title: Finite Element Investigation of Pre-Damaged RC Columns Retrofitted with FRCM

Date of Defense: 27/05/2021

Name, Title and Affiliation	**Signature**
Dr. Farid Abed Professor, Department of Civil Engineering Thesis Advisor	
Dr. Jamal Abdalla Professor, Department of Civil Engineering Thesis Committee Member	
Dr. Maen Alkhader Associate Professor, Department of Mechanical Engineering Thesis Committee Member	
Dr. Irtishad Ahmad Head Department of Civil Engineering	
Dr. Lotfi Romdhane Associate Dean of Graduate Affairs and Research College of Engineering	
Dr. Sameer Al-Asheh Interim Dean College of Engineering	
Dr. Mohamed El-Tarhuni Vice Provost for Research and Graduate Studies Office of Graduate Studies	

Acknowledgement

I would like to thank my advisor Dr. Farid Abed for providing opportunity and knowledge, guidance, support, and motivation throughout my thesis. I'm deeply beholden for his great assistance, worthy discussion, suggestions and patience.

I would like to thank the professors of the Civil Engineering department who taught me the master level courses with mighty teaching methods and skills. I really appreciate their dignified advice and motivation.

I would like to thank American University of Sharjah for supporting my studies and thesis with a Graduate Research Assistantship scholarship.

Dedication

To my family.

Abstract

Reinforced concrete (RC) structures in the UAE and globally face adverse deterioration during their lifetime. A novel retrofitting system using poly-paraphenylene-benzobisoxazole (PBO) Fiber Reinforced Cementitious Matrix (FRCM) is investigated in this thesis. FRCM is a noncorrosive two-dimensional high strength FRP mesh saturated with inorganic cement mortar which is compatible with concrete substrates. A three-dimensional (3D) nonlinear finite element (FE) model is developed using ABAQUS to study the behaviour of corrosion damaged RC columns retrofitted with PBO-FRCM systems. A total 180 cases of FE models are developed using a concrete compressive strength of 30 MPa and a longitudinal reinforcement ratio of 2% typical to columns. A comprehensive parametric study is conducted considering the effects of five parameters: (a) cross section type (square vs circular), (b) FRCM layers (1 vs 2 vs 3 vs 4 layers), (c) damage level (mild vs moderate vs severe damage), (d) eccentricity ratio (e/h= 0.0, 0.3, 0.5, 0.75, 1.0, 1.25 and 1.5) (e) column type/length (short/800mm vs slender/1200mm). Displacement controlled loading condition is used and material nonlinearities in concrete, cement mortar and composite are incorporated in the FE model. The FE models are validated against published literature. Results indicated a positive correlation between the number of FRCM layers, axial capacity, and ductility enhancement which is more pronounced in circular columns. Enhancement in axial capacity of 20% was observed in square columns and 35% in circular columns while axial ductility enhancement of 42% was observed in square columns and 164% in circular columns. All strengthened specimens failed by matrix damage indicating effectiveness of the strengthening system irrespective of the cross-section type. Retrofitting corrosion damaged RC columns with PBO-FRCM restored and enhanced the axial capacity and ductility at all damage levels. Increasing the number of FRCM layers increased the axial capacity of eccentrically loaded columns irrespective of damage level and eccentricity ratio. Comparison of column axial capacity, which was computed based on ACI 549.4R-13 provisions, against FEA revealed that the code provisions underestimate the axial capacity of short RC columns retrofitted with PBO-FRCM by 20%.

Keywords: Nonlinear FEA, FRCM, PBO-FRP, ABAQUS, Reinforced Concrete

Table of Contents

List of Figures

List of Tables

List of Abbreviations

FEA	Finite Element Analysis
FRCM	Fiber Reinforced Cementitious Matrix
FRP	Fiber Reinforced Polymer
PBO	Poly-paraphenylene Ben-zobisoxazole
RC	Reinforced Concrete

Chapter 1. Introduction

1.1. Background

Reinforced concrete (RC) is the most common construction material worldwide. In the UAE specifically majority of structures are predominantly made of reinforced concrete. This is a testament to the ease and speed of construction, durability, versatility and economic advantages of RC structures. Despite these advantages, deterioration of reinforced concrete (RC) structures over their service life is inevitable. The environmental conditions of the UAE (high temperatures, severe humidity, and high soil chloride content) favor accelerated corrosion rates of reinforcing steel bars in RC structures. Case studies proved that coastal structures suffer from extensive carbonation and chloride attack, causing reinforcement corrosion, cracks, and concrete spalling after 10 years of age [1]. A more recent study reported the surface chloride build up rate at 0.3% of concrete weight per year in tidal zone of the Arabian Gulf relative to 0.04-0.15% in other marine environments [2].

Majority of the RC structures in the region have been designed and constructed in the previous century prior to the latest additions to the current seismic design codes and therefore do not satisfy the necessary seismic requirements such as transverse reinforcement spacing, detailing and ductility. These structures are considered seismically unstable and are prone to severe structural damage beyond repair (financial loss) and high chance of collapse (loss of lives) during seismic activity especially as technology and research in this area has advanced. The combined threats of corroded reinforcement and seismic deficiency may lead to catastrophic consequences and therefore strengthening is required to ensure corrosion damaged structures are protect under service loading and during extreme events such as earthquakes.

Corrosion can be explained as a natural process that converts a refined metal into a more chemically stable form such as oxide, hydroxide, or sulfide. Corrosion is the gradual destruction of the reinforcing steel in reinforced concrete through a chemical reaction known as oxidation. This process is accelerated in the presence of moisture and oxygen. Corrosion causes crack formation and propagation in the concrete, and gradual reduction in the steel cross section and mechanical properties such as strength and ductility. Major concerns arise when corrosion occurs in the plastic

hinge regions of columns, where both strength and ductility are vital and cannot be compromised [3]. Once corroded, these regions fail to fulfill their expected role of energy dissipation during seismic activity, jeopardizing the entire structural integrity.

The cost of rehabilitation of RC structures is usually steep and therefore the need for a reliable technique to tackle the effects of corrosion is crucial for both researchers and practicing engineers. Conventionally, rehabilitation of corrosion damaged structures involves the replacement of the corroded bars and deteriorated concrete layers. In combination with seismic hazards, improved techniques need to be adapted to restore the seismic stability of the structure. In RC columns, which is the focus of this study, replacing the corroded bars is usually followed by additional confinement of the structurally deficient columns in forms of jacketing or wrapping. One of the most practiced techniques is strengthening with externally bonded fiber-reinforced polymers (FRP). FRP strengthening gained recognition as a result of its numerous advantages such as effectiveness in retrofitting damaged RC structures [4] [5], corrosion resistance and high strength to weight ratio.

1.2. Problem Statement

The efficiency of the externally bonded FRP in delaying the rate of corrosion of the reinforcing bars is questioned by the lack of research that investigates the post-repair performance of the FRP-retrofitted structures. Epoxy bonded FRP is highly flammable and prone to deterioration of their mechanical and bond properties at elevated temperatures [6] [7] [8]. This raises a great concern of feasibility of externally bonded FRP in the UAE where high temperatures prevail all year round. The toxic nature of epoxy and its poor thermal compatibility to the concrete substrate adds another dimension to the drawbacks of the use of epoxy bonded FRP systems in elevated temperatures. The UAE is significantly investing in modernized civil infrastructure, majority of which are predominantly reinforced concrete and located in a country that is disadvantaged with harsh environment causing reinforcement corrosion and exposure to seismic activity. Provisions for maintenance and reliable repairing schemes to ensure safe, uninterrupted, and efficient functionality of existing infrastructure is vital. The development of any modern society needs to address sustainability for its own welfare and to protect the planet at large. With these perspectives in mind, the need for an

optimum retrofitting technique that suits the prevailing conditions in UAE arises. The solution addresses the following:

1. The proposed solution provides human safety against possible risk of structural deterioration through retrofitting.
2. The proposed solution is sustainable in terms of functionality, integrity, and compatibility with the existing infrastructure with consideration of the harsh environment that prevails in UAE.
3. The proposed solution does not constitute human health risk among those implementing it, contrary to the health risks associated with epoxy based FRP retrofitting techniques.
4. The proposed solution considers that majority of construction work in UAE is a trowel-trade, which is compatible with the use of mortars in FRCM systems.

1.3. Objectives

A new retrofitting technique for RC structures considering the harsh environment that prevails in the region focusing on corrosion damage is investigated. The main objectives of this thesis are as follows:

1. Develop finite element models to simulate pre-damaged FRCM-retrofitted columns.
2. Using the developed models to investigate the confinement and slenderness behavior of corrosion damaged RC columns strengthened with 1, 2, 3 and 4 FRCM layers under concentric and eccentric loading.
3. Provide recommendations on modeling and application of FRCM on retrofitted RC columns.

This study aims to address the above objectives through integrating advanced aerospace-age material (fibers reinforcing polymer) with traditional materials (cementitious mortar) to form a novel composite known as the Fiber Reinforced Cementitious Matrix (FRCM) made possible by advances in materials science and nanotechnology. The potential of FRCM in retrofitting pre-damaged RC structures exposed to harsh environments stems from its mechanical performance, ease and

simplicity of application that does not require the retraining of construction workforce. This study aims to overcome the drawbacks of epoxy based FRP products by proposing an alternative that is user friendly, environmentally friendly, economically viable and most importantly an effective system. FRCM systems consist of one or more layers of non-corrosive textiles made of carbon, glass, or poly-paraphenylene-benzobisoxazole (PBO) grids that are sandwiched between layers of cementitious mortars. The process of FRCM retrofitting is presented in Figure 1. The cement-based mortar used in FRCM forms a protection shield against chloride ion penetration thus protecting the main reinforcing bars from corrosion attack. The characteristics of the proposed FRCM composite system such as lightweight, high tensile strength, and ease of application in addition to the fire resistance capabilities of the cementitious mortar layers through shielding the embedded fibers and minimizing its vulnerability hazard makes it extremely appealing over epoxy bonded FRP system. The compatibility between the cementitious mortar and the concrete substrate is inherent as both materials have a common cement "base", adding to the various mentioned advantages of FRCM systems. FRCM systems, with their innovative features, ensure the endurance of the rehabilitation process and consequently the sustainability of the repaired structure.

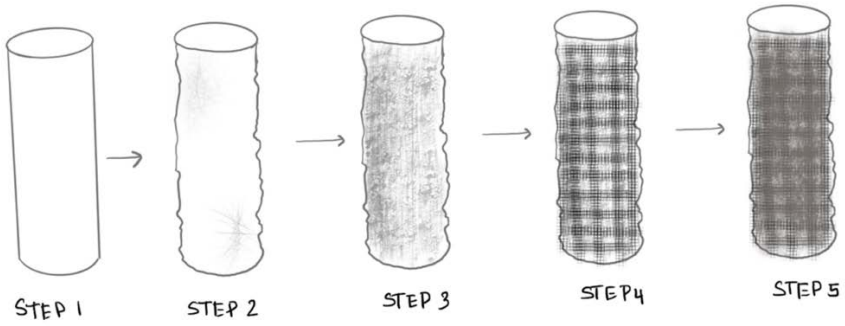

Figure 1: FRCM Application Scheme

Step 1: Damaged RC Column

Step 2: Surface Preparation (water jet or sand blasting)

Step 3: First layer of mortar application

Step 4: Textile Impregnation

Step 5: Second layer of mortar application

Chapter 2. Literature Review

The use of FRCM to repair existing structures is gaining recognition. The following section highlights the success and limitation of the system in a variety of applications.

2.1. Corrosion Protection and Repair

Su et al. [9] investigated the effects different types and volumes of high molecular weight polymer such as re-dispersible polymer powder and styrene butadiene latex on the flexural, shear, compressive strength and conductivity. The authors also investigated varying the amounts of chopped carbon fiber and impressed current density. The authors discovered that using chopped carbon fibers can provide effective cathodic protection for reinforcement in RC structures. Furthermore, the authors observed that as the current density increased the shear strength between the C-FRCM and concrete substrate decreased as a result of anodic polarization. C-FRCM composite (carbon-fiber-reinforced cementitious matrix) also serves as a dual-functioning material for the combined cathodic protection and structural strengthening of reinforced concrete structures in chloride exposed environments for a reasonably long period. El ghazy et al. [10] studied the effects of different FRCM types by subjecting the beams to accelerated corrosion process to obtain a steel mass loss of 10% and 20% and varying the type of FRCM composites and the number of FRCM layers applied. The study concluded that the use of strengthening composites did not affect the beam stiffness prior to yielding. The strengthening system was also able to restore original capacity of the corrosion-damaged beams. However, the level of enhancement in the strength depended on the amount and type of FRCM regardless the severity of the damage. In a similar study by the same author [11] varying the fabric types, schemes and number of layers confirmed that increasing the number of FRCM layers increased both the yield and ultimate loads consequently increasing the ductility index. The results also showed that the use of continuous u-wrap strips was more effective than end-anchored. PBO-FRCM was able to restore 105-144% of the original capacity and ductility index of the corroded specimens.

EL ghazy et al. [12] investigated further the effectiveness of using FRCM composites in strengthening corrosion damaged RC beams using different schemes (U-shaped transverse strip bonded around the cross-section or bottom flexural strips with

U-shaped continuous ply wrapped along the beam span). Several FRCM plies were studied and results revealed two distinct failure modes: slippage and delamination of the fabric within the matrix. Increase in both ultimate and yield strength with increase in number of plies was noticed for specimens repaired with scheme 1, however ductility was decreased. Scheme 2 was more efficient in improving the strength of the beam in terms of both yield and ultimate.

2.2. Masonry Column Confinement

Murgo, and Mazzotti [13] studied the structural behaviour of masonry columns strengthened with FRCM using a modified version of Spoelstra-Monti's iterative approach for FRP-confined concrete columns combined with a modified version of Mander's model with the assumption that the transverse confining pressure provided by the stirrups on the concrete core would be constant and corresponding to its maximum value. Spoelstra-Monti considered the increasing confining action by using an iterative-incremental process. A 1D model was used to introduce the confining effect in a simple yet effective way and a 3D model was used for validation. The authors also experimentally strengthened masonry columns and varied the type of FRCM (glass or carbon-FRCM), rounding corners of the specimens and anchorage bond length. They deduced the mechanical characterization of the masonry specimens by using slightly destructive and destructive tests. The results showed a slightly higher initial stiffness with non-linear behaviour initiating earlier, at about 40% of the peak load in columns wrapped with FRCM. Columns wrapped with carbon grids showed a mean capacity 5% higher than columns wrapped with glass grids. The authors concluded that little amounts of FRCM could impact the confinement capability of the wrapping system. Moreover, it was noticed that rounding the corners led to an earlier failure mode and fiber buckling is the dominating failure mode.

2.3. Flexural Strengthening

Elghazy et al. [14] investigated post-repair flexural performance of corrosion-damaged beams strengthened with different FRCM composites by comparing PBO-FRCM Carbon-FRCM with the following schemes: scheme 1 is anchoring each end with one U-shaped transverse strip and scheme 2 is wrapping the FRCM composites with a U-shaped continuous ply along the beam length. The results showed that beams repaired with scheme 1 had higher percentage of mass loss than beams repaired with

scheme 2. Crack patterns highly depend on the FRCM composite and the repairing scheme. Three different failure modes observed: FRCM delamination, partial debonding of the fabric, and flexural cracking. Scheme 2 impacted the modes of failure irrespective of the FRCM material because premature delamination of FRCM was prevented. Moreover, the U-wrapped scheme delayed the delamination of the FRCM in the short-term beams making it more effective than the end anchoring scheme. However, long term beams repaired with scheme 2 showed higher ductility index and energy absorption. The PBO-FRCM repaired beams showed lower post-yielding stiffness and more ductility at failure than those of their carbon-FRCM repaired counterparts. El Ghazy et al. in a similar study [15] further concluded that the use of PBO-FRCM demonstrated higher strength increase ranging between 7% and 44% relative to the specimens strengthened with carbon-FRCM. Furthermore, the strengthened beams had ductility indices between 86% and 118% and energy absorption indices between 111% and 153% of that of the original beam.

Another study by Jabr et al. [16] varied the steel reinforcement ratio in reinforced concrete beams. Beams with of low (0.18) and moderate (0.36) steel reinforcement ratios strengthened with 2 plies of PBO-FRCM, carbon-FRCM and Glass-FRCM were investigated. The results concluded that PBO-FRCM significantly enhanced the ultimate capacity of the strengthened beams compared to glass and carbon-FRCM irrespective of reinforcement ratio. Furthermore, both carbon and glass FRCM did not significantly impact the ultimate load capacity due to premature failure in the FRCM. Carbon-FRCM showed the greatest increase in the post-cracking stiffness, around 23% and increased the yielding load by 17% and decreased the deflection at that point. FRCM also reduced the crack width relative to the un-strengthened control beam.

Sneed et al. [17] studied the behaviour of strengthening reinforced concrete with steel-FRCM through varying 3 parameters; number of FRCM layers, installation type (u-wrap vs anchorage) and the loading rate. The authors tested seven specimens using a single-lap shear test and concluded that lowering the concrete compressive strength and decreasing the concrete cover decreased the load-carrying capacity and that failure of FRCM strengthened beams was primarily governed by the fabric slippage within the matrix. Furthermore, it was noticed that failure mode of C-FRP and P-FRCM

strengthened beams is independent of corrosion level. In addition, all beams strengthened with 2 and 4 layers had the same failure mode (delamination of the FRCM layer at the matrix interface) regardless the corrosion level. The authors concluded that C-FRP was more efficient in restoring and increasing the load-carrying capacity of the corrosion damaged beams with a similar axial stiffness as P-FRCM, yet P-FRCM is still a good approach to restore/increase the load-carrying capacity.

2.4. Fatigue/Seismic Retrofitting

Hadad et al. [18] investigated the fatigue performance of FRCM-strengthened reinforced concrete beams through varying the type of fabric (bidirectional and unidirectional carbon fabric) and the loading type (either static/monotonic loading or fatigue/cyclic loading). The static loading was induced in form of displacement control, whereas fatigue loading was in force control mode. Results of the static tests indicated that the effect of FRCM stiffness was more visible after cracks developed and the strengthened specimens showed a higher post-cracking stiffness than that of the un-strengthened counterparts. FRCM-strengthened beams failed by interlaminar delamination at the fabric-matrix interface. Debonding of FRCM was not observed. The results from the fatigue tests showed that SEM confirmed that the fatigue fracture of both strengthened and un-strengthened beams failed mainly due to yielding of the reinforcing steel bars.

Pino et al. [18] investigated the behaviour of the strengthened beams as they were being subjected to static and cyclic loading. The authors varied the amount of supplemental reinforcement, ultimate strength, and the applied stress range. The specimens were divided into 2 phases, where the first phase included 5 specimens tested monotonically until failure and 4 quasi-static loading and unloading cycles followed by a final displacement-controlled load up till failure. In the second phase, 10 specimens were subjected to cyclic fatigue loading resembling a sine wave. A 33% increase in the design strength was observed in 6 out of the 10 specimens that were selected for phase 2. The results for the specimens in the first phase were similar up till cracking. The post-cracking stiffness was enhanced in all beams strengthened with FRCM compared to the un-strengthened beam. However, the cracking load wasn't significantly impacted by the FRCM. The failure modes varied based on the number of FRCM layers. The results for the specimens in the second phase showed that the beam specimens that were

strengthened with 3 layers of PBO-FRCM were subjected to a higher load and experienced a shorter fatigue life. However, the fatigue behaviour was divided into 3 levels where at the initial stage a considerable damage is noticed, at the second stage the damage happens steadily and gradually and lastly at the final stage a significant loss in the strength is observed followed by a sudden FRCM delamination. All strengthened beams showed that the main failure mode was due to the fatigue rupture of steel reinforcement. However, the secondary failure mode was due to the fabric slippage within the matrix, or FRCM delamination as it was noticed that the secondary failure was a function of the amount of FRCM reinforcement.

Faleschini et al. [19] studied severely damaged reinforced concrete joints were strengthened with FRCM and FRP. One specimen was strengthened with FRCM while the other 2 specimens were strengthened with FRP in two different orientations. The results are summarized in terms of load-carrying capacity, stiffness deterioration, ductility, dissipated energy, and equivalent viscous damping ratio. The results indicated that the FRCM strengthened specimen developed vertical, horizontal and diagonal cracks in the joint panel region with varying widths, attaining 84% of the load carrying capacity of the original specimen. The energy dissipated by the repaired specimen was up to 70% of the original specimen. Whereas the results of the FRP strengthened specimen attained peak loads of 79% and 70% of the original specimen under the push and pull conditions, respectively. High stress levels concentrated in the panel joint led to fracture of the diagonal fibers. The peak loads in the third specimen were 65% & 76% of the capacity of the original specimen under the push and pull conditions, respectively. It was noticed that the fibers have provided significant improvements to the specimen in terms of bending strength during the pull loading phase. Furthermore, the repaired specimen dissipated 58% of the energy dissipated by the original specimen.

2.5. FRCM Bond

Younis and Ebead [20] investigated the bond characteristics of FRCM by varying the fabric type, bond length, and the number of FRCM plies applied. FRCM systems were applied to both sides of the 18 concrete specimens to obtain a double shear connection. Three different failure modes for each FRCM type were observed. Carbon-FRCM showed fabric debonding within the fabric interface at failure. PBO-FRCM exhibited debonding at the concrete interface at failure. Glass-FRCM showed

premature rupture. Moreover, it was noticed that the effect of increasing the number of layers depended on the type of the FRCM. Increasing the bond length increased the bond capacity in all FRCM types, and a higher bond capacity was observed in PBO-FRCM than both carbon and glass FRCM. Carozzi and Poggy [21] performed an experiment to understand the behaviour of the FRCM materials and their properties, focusing on 4 different types of FRCM (PBO, Carbon-FRCM, Glass-FRCM, PBO and Glass). The authors applied cyclic loading and push-pull double lap tests. The results revealed that the bond length impacted the failure load and mechanism of all FRCM types except PBO-G-FRCM. Increasing the bond length increased the failure load through preventing debonding. Specimens have shown different failure modes based on the FRCM type; Glass-FRCM exhibited slippage at small loads followed by a partial failure; PBO and carbon-FRCM showed a similar failure mode, which was a progressive failure of the roving and no slippage; PBO-G-FRCM failure mode was characterized by the collapse of the glass fibers followed by a gradual failure of the PBO fibers in the weft and warp directions. The authors concluded that PBO was the best strengthening FRCM type as it had the best overall performance.

2.6. Axial Strengthening

Limited sources investigated the use of FRCM strengthening systems in axial strengthening Ombres and Verre [22] investigated the effects of varying the reinforcement ratio and the eccentricity-to-section height ratio. The specimens were subjected to eccentric loading. Single and double layers of PBO-FRCM were used in the specimens. The authors concluded that the ultimate strength of the confined specimens for both single and double layers of PBO-FRCM decreased with increasing eccentricity. Additionally, the authors observed significant improvements in the ductility of the specimens and failure modes observed throughout the experiment were highly dependent on the confinement ratio. Varying the eccentricity value had no impact on the failure mode.

Colajanni et al. [23] studied the uniaxial behaviour of different beam geometries (circular and square cross-sections) strengthened with varying layers of FRCM. The results for the circular cross-section strengthened specimens showed an increase in strength of 19% & 33% for 2 & 3 layers respectively. All specimens experienced a reduction in axial stiffness after the first peak stress and failed as a result of the

telescopic jacket textile failure, which occurred as a result of the wide vertical cracks in the textile overlapping region. Furthermore, strength increase of 23% was reported for 0.236% confinement ratio. The results of the square cross-section showed that hardening behaviour in the post peak branch was achieved as expected as the confinement volumetric ratio was low (0.175%). In addition, the wrapping system ensured a ductile behaviour. In comparison, the increase in the ultimate strain in the square cross-section specimens were lower than the circular cross-section specimens by about 20%. However, PBO-FRCM improved the ductility and compressive strength in the concrete beams significantly and was found to improve the axial deformability in square cross-sections. Another important point is using a cementitious mortar instead of resin-impregnated system delayed the activation of the confinement system, and the post peak stiffness degradation was immediately retrieved.

Parretti and Nanni [24] conducted tests to check circular and rectangular concrete columns with unidirectional CFRP wraps oriented in 45 degree and hoop directions. It was found out that the ultimate strength attained using 45-degree laminates was less than that in the hoop direction. However, the ductility was higher in the 45-degree laminate application because of the enlargement of failure planes causing higher amounts of energy dissipation. Suggestions were made for changes in design guidelines based on these results. Esfahani et al. [25] experimentally studied the axial strength of six circular and square columns with varying corner shapes that were confined with CFRP wrapping. It was found that CFRP notably increased the strength and ductility of both column types and correlated well with code provisions. Square columns with rounded and sharp corners performed similarly. Obaidat [26] developed a 3-D nonlinear finite element model framework for concrete beams strengthened with CFRP laminates using material models from literature and compared the results to experimental values obtained. It was found that as the length of FRP increased the beam flexural and shear strengths also increased. FRP to concrete ratio and the FRP stiffness affected the failure mode of the specimens. Additionally, ACI 549.4R-13 [27] design guidelines are capable of predicting the capacity and the failure mode of the specimens, however there are limitations. Since micromechanics of composite material are complex and experimental investigations are time consuming, finite element modeling (FEM) can be conveniently used for this purpose [28].

Chapter 3. Methodology

Analysis of externally bonded FRCM strengthening systems on concrete columns presents several challenges due to composite action of the different components (concrete; steel; FRP). This analysis is highly nonlinear in nature and therefore presents complications that can result in convergence problems. A simplified yet accurate numerical approach in which suitable numerical models are adapted for each material using established laws and mechanics, and the interaction between the different materials is defined. The properties of each material interaction between FRCM and concrete incorporated in the FE model are presented in this section.

3.1. Material Properties and Constitutive Models

3.1.1. Concrete. Concrete compressive behaviour is linearly elastic until initiation of micro cracking which then induces nonlinear behaviour until ultimate compressive strength is achieved, followed by decreasing strength with increasing strain. Concrete behaviour under uni-axial tension is initially a linear elastic relationship until failure stress (corresponding to the onset of micro-cracking) is achieved. Softening then occurs with a sudden brittle failure path as shown in Figure 2.

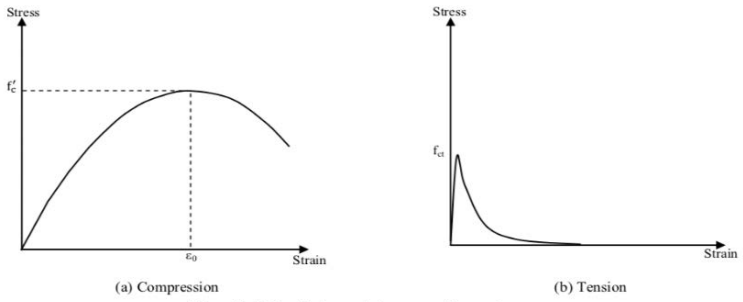

Figure 2: Concrete Behaviour in Tension and Compression [1]

Several approaches with varying level of complexity can be used to characterize concrete behaviour. A constitutive model for concrete behaviour is selected based on the ability of the model to capture the mechanical behaviours such as softening, crack formation/propagation and concrete damage. A popular approach is the discrete crack model, in which the cracks are defined along element boundaries and the compressive concrete response modelled by Drucker-Prager perfect plasticity. The smeared crack model approach is based on the premise that cracking of concrete occurs when the principal tensile stress exceeds the tensile strength. The elastic modulus of the material

is then assumed to be zero in the direction parallel to the principal tensile stress direction [26]. The third approach is a plastic damage model. Plastic damage models have been successful in predicting the response of standard concrete tests in both tension and compression, attributing the nonlinear material behaviour of concrete to two distinct material mechanical processes; plasticity and damage mechanisms. Hardening variables are used to represent the damage in concrete and stiffness degradation is evaluated to represent the uni-axial tensile and compressive stress-strain response. Tensile cracking and compressive crushing are assumed to be the main two failure mechanisms of the concrete material [26].

Abaqus integrated two approaches in their commercial software package to predict the behaviour of concrete: smeared crack and plastic damage models. The concrete damaged plasticity (*CDP*) model is defined by two main concrete failure mechanisms i.e., cracking under tension and crushing under compression and four further dimensionless parameters. *CDP* therefore possesses a high convergence potential and is adapted in this thesis. The *CDP* consists of a modification of the traditional *Drucker-Prager criterion* based on isotropic damage development. Continuum damage mechanics and stiffness degradation are used to model the crack propagation [26]. The plastic damage model requires the input of elastic modulus, Poisson's ratio, plastic damage parameters and a description of compressive and tensile behaviour from constitutive models. The dilation angle is the angle of internal friction of concrete material and oscillates between 30° to 40°, the flow potential eccentricity is a small positive number that defines the rate at which the hyperbolic flow potential approaches its asymptote, fb0/fc0 parameter represents the ratio between the concrete compressive strength in biaxial state and the concrete compressive strength in uniaxial state, k is the ratio of the second stress invariant on the tensile meridian to that on the compressive meridian, and the viscosity parameter defines visco-plastic regularization. Poisson's ratio is defined as 0.2. The five plastic damage parameters recommended by the Abaqus manual [29] for defining concrete material are presented in Table 1.

Table 1: CDP Behavioral Model Parameters

CDP Behavioral Model Parameters				
Dilation Angle	Eccentricity	fb0/fc0	k	Viscosity
30	0.1	1.16	0.667	0.001

Additionally concrete compressive and tensile behaviour constitutive models, along with plastic damage models published in literature [26] are defined. This model assumed two basic concrete failure mechanisms, compressive cracking and tensile softening. The concrete modulus of elasticity is given by equation 1:

$$E_c = 4700\sqrt{f'_c} \tag{1}$$

where E_c is the concrete elastic modulus and f'_c is the concrete compressive strength in MPa. The stress-strain response is generated using the equation 2 [26]:

$$\sigma_c = \frac{E_c \varepsilon_c}{1+(R+R_E-2)\left(\frac{\varepsilon_c}{\varepsilon_0}\right)-(2R-1)\left(\frac{\varepsilon_c}{\varepsilon_0}\right)^2+R\left(\frac{\varepsilon_c}{\varepsilon_0}\right)^3} \tag{2}$$

where:

$R = \frac{R_E(R_\sigma-1)}{(R_E-1)^2} - \frac{1}{R_E}$, $R_E = \frac{E_c}{E_0}$, $E_0 = \frac{f'_c}{\varepsilon_0}$,

$\varepsilon_0 = 0.003$ $(ultimate\ compressive\ strain)$

$R_\sigma = 4$, $\nu = 0.2$ $(poisson's\ ratio)$

The resulting concrete compressive stress-strain curve is shown in the Figure 3 below:

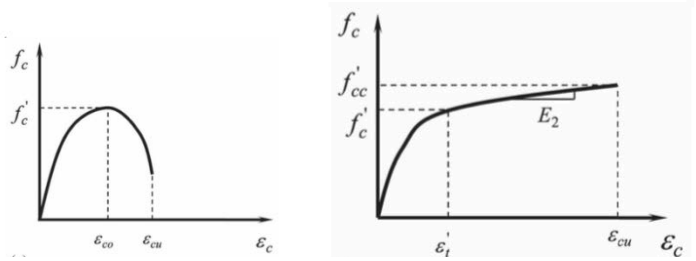

(a) (b)

Figure 3: (a) Unconfined Concrete Model (b) Confined Concrete Model [30]

Inelastic strain (ε_{in}) can be calculated from total strain using equation 3:

$$\varepsilon_{in} = \varepsilon_c - \varepsilon_0 \tag{3}$$

Under uniaxial tension, the concrete response is assumed linear elastic until the failure stress is achieved. The equation below was used to develop the pre-peak tensile response:

$$f'_{ct} = 0.33\sqrt{f'_c} \tag{4}$$

where f'_{ct} is the tensile strength and f'_c is compressive strength in MPa.

To define the post-peak tensile failure behaviour of concrete, the model used the fracture energy method, defined as the area under softening curve (assumed as 90 J/m2) [26].

3.1.2. Reinforcing steel. Steel behaviour follows an initial linearly elastic zone proportional to the elastic modulus until the yield stress, where nonlinear behaviour begins until the ultimate tensile stress is achieved. Necking of the steel begins after ultimate point and complete fracture occurs at maximum strain. A typical stress-strain response for reinforcing steel is shown in Figure 4.

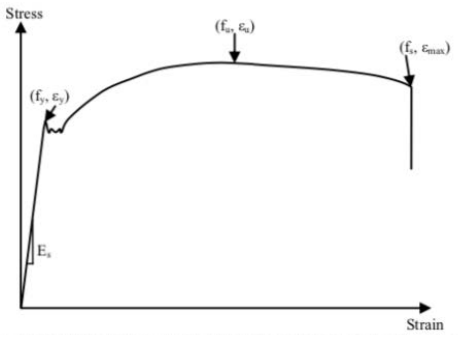

Figure 4: Typical Stress-Strain curve for reinforcing steel [1]

An elastic-plastic behaviour, with or without strain hardening, is an acceptable approximation for steel in modelling applications. The steel reinforcement is considered to behave as an elastic-perfectly plastic material identical in tension and compression [26] in this thesis. Poisson's ratio of 0.3 is used with elastic modulus and yield strength of 200 GPa and 500 MPa, respectively. Figure 5 shows an idealized steel stress-strain curve.

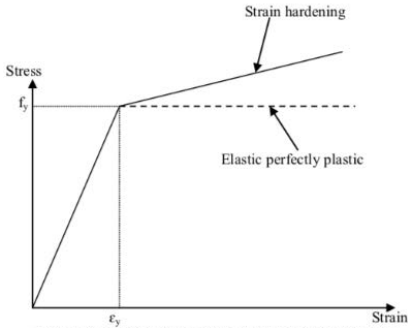

Figure 5: Idealized Stress-Strain Curve for reinforcing steel [1]

3.1.3. FRCM composite. FRCM is made up of high strength FRP fibers impregnated in cementitious mortar that is compatible with concrete substrates. The fibers provides load bearing capacity and stiffness to the composite while the mortar distributes the load between the fibers, ensures composite action and protects the fibers from harsh environment. The most common FRP in engineering applications are glass, carbon, aramid and poly-paraphenylene-ben-zobisoxazole (PBO). Carbon fibers have the highest stiffness, most durable and most expensive. Carbon also endures harsh environments. Glass fibers are cheaper but have lower strength and significantly lower stiffness. Unprotected glass fibers also degrade in most harsh environments. Aramid fibers have mechanical characteristics in between glass and carbon [26]. All these fibers behave linearly elastic until failure. PBO-FRCM is used as the strengthening FRP in this thesis as it has the best overall performance [21]. Linear elastic behavior until failure is defined for PBO FRP with elastic modulus 270 GPa and tensile strength 5800 MPa [31]. Orthotropic behavior is usually defined for FRP however since this mesh is interwoven bidirectionally, isotropy is assumed. Confinement resulting from number of FRP layers is incorporated in the model in form of confined compressive f'_{cc} computed using equation 5 recommended by ACI 549.4R-13 [27]. The cementitious mortar used to bond the fibers to the column surface is compatible with concrete substrates and the strengthened element undergoes surface preparation (sand blasting and cleaning) therefore perfect bond is assumed between FRCM and concrete column. Compressive strength of 30MPa is used for the mortar which is assumed to crack under slight loading due to its negligible thickness. Perfect bond at steel to concrete interface is also assumed in this study. Table 2 shows the material properties of PBO FRCM adapted in the model. Figure 6 shows the PBO-FRCM used herein.

Figure 6: PBO-FRCM

Table 2: FRCM Material Properties

Material Property		PBO fiber mesh	Cement based matrix	PBO-FRCM system [31]
Tensile Strength	(MPa)	5800	na	1664
Compressive Strength	(MPa)	na	30	na
Young modulus	(Gpa)	270	6	128
Failure strain	(%)	2.00	na	1.7565
Nominal thickness	(mm)	0.0455	na	

$$f'_{cc} = f'_c + \psi_f 3.3 \kappa_a f_1 \tag{5}$$

$$f_1 = \frac{2E_f n A_f \varepsilon_{fe}}{\sqrt{b^2+h^2}} \ , \varepsilon_{fe} = \varepsilon_{fe} \ or \ 0.012 \tag{6}$$

$$f_1 = \frac{2E_f n A_f \varepsilon_{fe}}{D} \ , \varepsilon_{fe} = \varepsilon_{fe} \ or \ 0.012 \tag{7}$$

$$\frac{A_e}{A_c} = \frac{1 - \frac{\left[\left(\frac{b}{h}\right)(h-2r_c)^2 + \left(\frac{b}{h}\right)(b-2r_c)^2\right]}{3A_g} - \rho_g}{1-\rho_g} \tag{8}$$

$$\kappa_a = \frac{A_e}{A_c}\left(\frac{b}{h}\right)^2 \tag{9}$$

$$\varepsilon_{fe} = \kappa_\varepsilon \varepsilon_{fu} \tag{10}$$

$$\kappa_\varepsilon = 0.55 \tag{11}$$

where:

A_g *is the gross cross sectional area*

A_e *is the effective confined area*

A_c *is the net cross sectional area*

A_f *is the mesh per unit width area*

b is the short dimension on a rectangular section

h is the long dimension on a rectangular section

D is the diameter of a circular section

r_c *is the radius of the edges on a rectangular section*

ρ_g *is the ratio of longutudinal steel to cross sectional area*

f'_c *is the compressive strength*

f'_{cc} *is the axial confined concrete compressive strength*

$\psi_f = 0.95$ *(strength reduction factor based on committee's judgement)*

κ_a *is the FRCM reinforcement efficiency factor*

f_1 *is the confinement pressure due to FRCM strengthening*

n *is the number of layers of mesh in FRCM*

E_f *is the tensile modulus of elasticity of FRCM*

ε_{ccu} *is the ultimate confined concrete axial compressive strain (from FEA)*

ε_{fe} *is the effective strain level in the FRCM at failure*

3.2. Finite Element Model Development

Commercial software package ABAQUS [29] is used to develop a nonlinear finite element model to simulate the behaviour of FRCM retrofitted RC columns. Modelling assumptions published in literature [26], [32] and [33] are adapted for this thesis.

3.2.1. Model geometry and element types. The columns are modelled using three dimensional simulations to gain overall understanding of the behaviour of the FRCM strengthened columns. No symmetry is assumed as nonlinear damage propagation is monitored throughout the concrete column to observe the failure mode.

The embedded reinforcing steel is modelled using a standard two-node 3D wire truss element **T3D2.** The steel properties are defined through the mass density, the elastic Young's modulus, Poisson's ratio, and yield stress since elastic perfectly plastic behaviour of steel is assumed in order to minimize convergence problems. Concrete is modelled as standard extruded 3D stress hexagonal element, an 8-node linear brick element with reduced integration **C3D8R**. Concrete behaviour is defined using concrete damaged plasticity parameters, formulated compressive and tensile behaviour as per the constituent models mentioned in section 3.1.1 of this study. Concrete compressive and tensile damage parameters are also defined accordingly amongst Young's modulus and Poisson's ratio. Compressive behaviour and compressive damage are defined using compressive models from published literature [26][28] mentioned in section 3.1.1. Tensile behaviour and tensile damage are assumed to be linear for static loading conditions to reduce convergence problems.

FRCM is modelled in two distinct parts, the FRP and the matrix. FRP is modelled using a standard four-node extruded thin shell element with reduced integration **S4R**. Material properties are defined using elastic engineering constant properties by defining the properties of the FRP constituent, Hashin damage using alpha as 1 and other parameters that include the mass density of the FRCM material. The FRP is assembled using composite layup option where the option of conventional shell and number of FRCM ply is selected with layer thickness of 0.5mm. Rotation angle of 90 degrees is selected which defines the direction of fibres along the direction of the hoops/ties. The matrix can be modelled using two approaches, cohesive element, or

cohesive surface. Both options were considered however when using cohesive surface, separation between the FRCM and concrete surface occurs due to wrinkling for the FRCM resulting from axial shortening of the column during the analysis. This interrupts the analysis when the ultimate load is reached creating another type of non-convergence therefore cohesive element was selected to model the matrix in this study. The matrix is modelled using standard 8-node 3D cohesive element **COH3D8** shown in Figure 7.

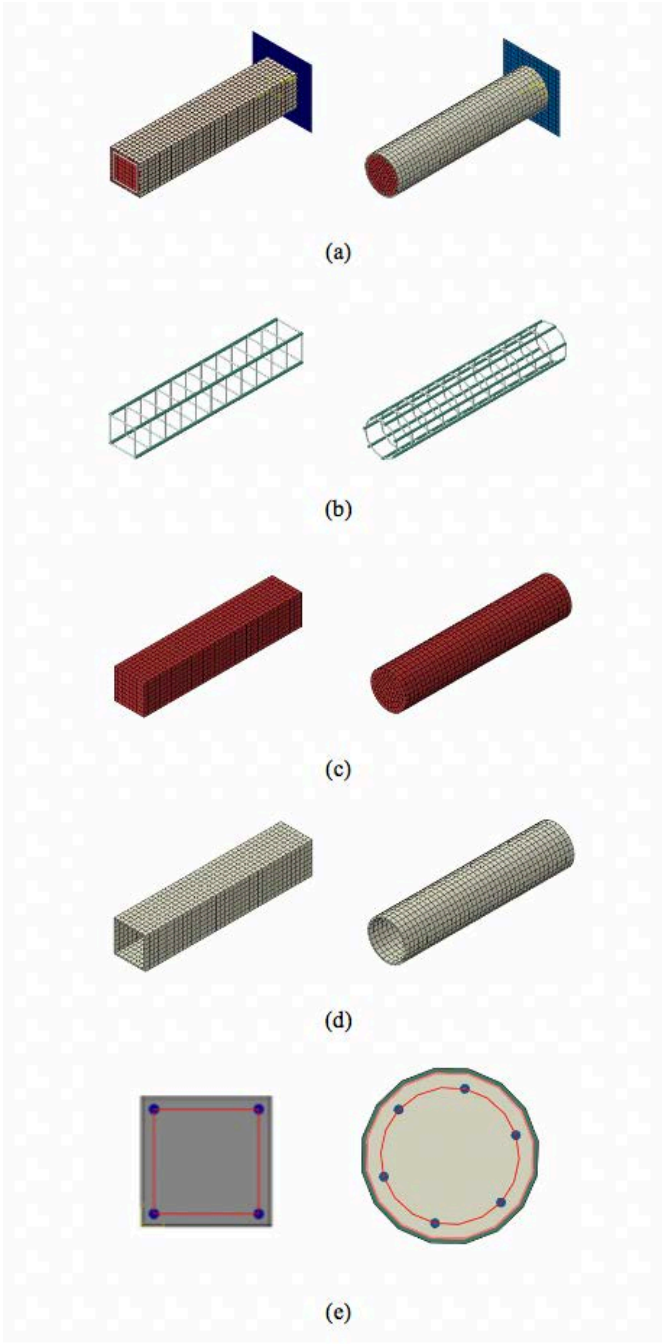

Figure 7: Model Geometry & Assembly (a) Column Assembly (b) Steel Reinforcement (c) Concrete (d) FRP & Matrix (e) Model Section

3.2.2. Boundary conditions & constraint. The fixed end of the column is defined though fixing all displacements and rotations using the ENCASTRE option in the concentric model while rotation is unrestrained in the eccentric model. The same boundary condition is used to hold the FRP and matrix system in place. A displacement boundary condition in which all displacements and rotations except U3 are restrained is applied to the reference point on the rigid plate for the concentric model while U3 and all rotations are unrestrained in the eccentric model. The steel reinforcement is constrained in the concrete using the embedded region constraint.

A tangential behaviour contact property with friction penalty formulation with friction coefficient of 0.1 is defined between the matrix and the column to simulate the bond between the column and the matrix. The matrix however has negligible thickness and is expected to be damaged during the analysis therefore tie constraints are assigned to ensure that the forces in the column are transmitted to the FRP smoothly if/when the matrix is damaged. Defining the FRCM in this way ensures that the same effects experienced in real life such as wrinkling of the FRCM due to axial shortening do not interrupt or terminate the analysis. Two tie constraints are assigned, one between the concrete column and the cementitious matrix defining the concrete as the master and the matrix as the slave and the second between the matrix and the FRP shell defining the matrix as the master and the FRP shell as the slave. The tie constraints will ensure that the analysis continues even when the matrix or the FRP is partially or fully damaged. Perfect bond between concrete and reinforcing steel is considered in the FE model.

3.2.3. Loading condition & pre-damage. Static loading condition is modelled by applying a linearly increasing displacement of 10mm with 1 second time period and 0.001 step increment. The infinitesimal increment will ensure a smooth step displacement-controlled analysis to determine the peak load and post-peak load behaviour of the column. Rigid Body and control point are assigned for the end plates to avoid premature failure at the ends of the column. The three levels of corrosive pre-damage, mild, moderate, and severe are modelled as percentage loss in steel reinforcement yield stress of 30%, 50% and 70% respectively.

3.2.4. Mesh configuration. Mesh sensitivity analysis was conducted on circular and square specimens using mesh sizes of 5, 10, 15, 20, 25, 30, 40 and 50mm.

The investigation revealed that finer mesh (5, 10 and 15mm) require heavy computational effort for negligible benefit in accuracy while coarser mesh (30, 40 and 50mm) compromised accuracy by up to 18% when compared to the experimental specimen. Mesh size between 15mm to 25mm for the concrete, FRP shell and matrix is optimal as it yields acceptable results with about 5% deviation and reasonable computational time. Time period of 1s was selected in this study however 10s is recommended for good computers. Mesh size of 20mm was selected throughout this study as it yielded average computational time of 3 to 4 hours depending on the number of FRCM layers and deviation in axial capacity of 2% for square specimens and 3% for circular specimens. Figure 8 and Table 3 below present a summary of the mesh sensitivity analysis.

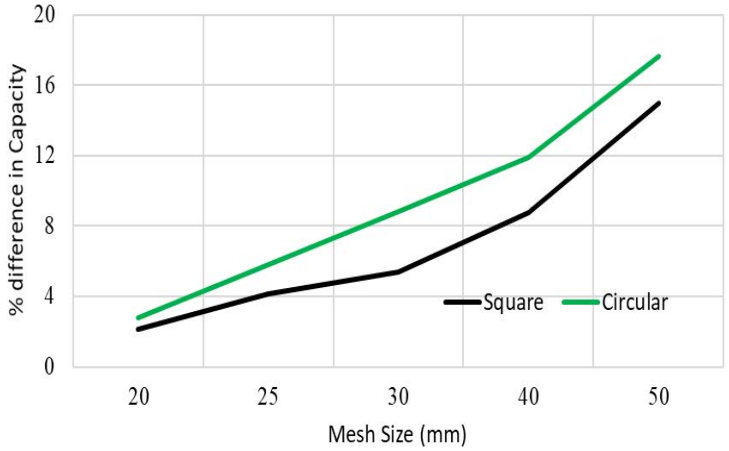

(a)

(b)

Figure 8: (a) Axial Capacity Deviation vs Mesh sizes (b) Mesh sizes used in Sensitivity Analysis

Table 3: Mesh Sensitivity Analysis

	Mesh Size (mm)	Pn (kN)	% Difference	Computational Time (hrs)
Circular	20	891	3	4
	25	897	6	2
	30	927	9	2
	40	959	12	1
	50	1026	18	1
Square	20	787	2	4
	25	792	4	2
	30	802	5	2
	40	832	9	1
	50	893	15	1

3.2.5. Convergence problems. The nonlinear behavior of the concrete material is accounted for in the modeling by introducing the actual plastic properties of the concrete in the model mentioned in section 3.1.1. Nonlinear analysis (NLGEOM) option is activated to account for large deformations and the P-delta effects in the eccentric columns. Despite these simplification assumptions, convergence difficulties appear when cracks start to initiate. Many approaches were adapted to ensure convergence such as using small time increments, reducing mesh size in the cohesive matrix, assigning tie constraint for the cohesive element to ensure analysis continuity and increasing the number of attempts at each step from the software default 5 attempts to 50 attempts per step increment.

3.2.6. Model verification. Results from three published literature presented in Figure 9 below are used to verify the FE model. Yazdani et al. [28] studied the behaviour of short RC columns strengthened with different layers of C-FRCM under concentric loading as shown in Figure 9(a). Tello et al. [31] investigated the behaviour of square and circular short RC columns strengthened with PBO-FRCM shown in Figure 9(b). These two studies are used in conjunction to verify the FE models developed for concentric columns in Series I of this study. Ombres et al. [22]

investigated eccentrically loaded columns shown in Figure 9(c) which are used as benchmark to validate the eccentrically loaded finite element models in Series II.

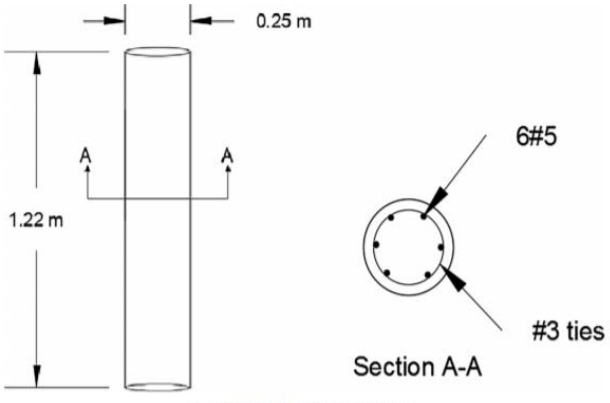

(a)

(b)

(c)

Figure 9: Experimental specimens used in model verification (a) Yazdani et al. [28] (b) Tello et al. [31] (c) Ombres et al. [22]

Further validation is conducted by comparing the failure modes of the modelled specimens from the FEM against results obtained by Tello et al. [31]. From figure 10(a), it is visible that the control specimens failed by concrete crushing and spalling in both square and circular specimens. The failure mode obtained through FEM is consistent with experimental findings. Furthermore, from Figure 10(b), the circular specimen failed by matrix damage at the bottom third of the column while the square specimen failed by damage of matrix in FRCM at the corners and bulging on the column sides. These findings are consistent with the experimental results.

Table 4: Model Verification

Column ID	Pu FEM (kN)	Pu Exp (kN)	% Difference
S0-0-0-SH	740	722	2
S0-0-1-SH	787	759	4
S0-0-2-SH	872	821	6
S0-0-4-SH	896	847	5
C0-0-0-SH	702	687	2
C0-0-2-SH	891	845	5
C0-0-4-SH	964	935	3
e30 1 layer	724	707	2
e30 2 layers	767	734	4
e50 2 layers	638	621	3
		Average	4

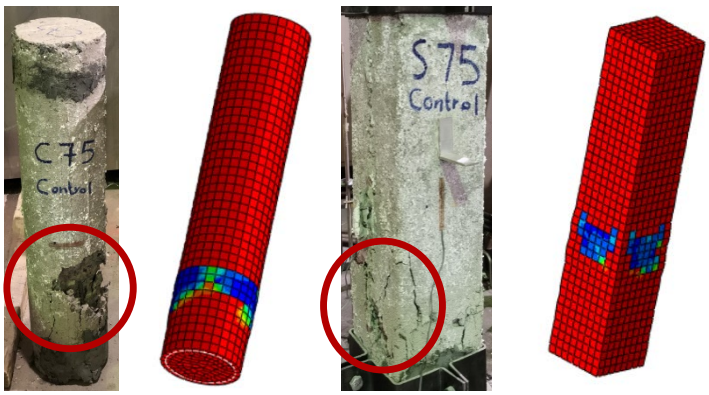

(a)

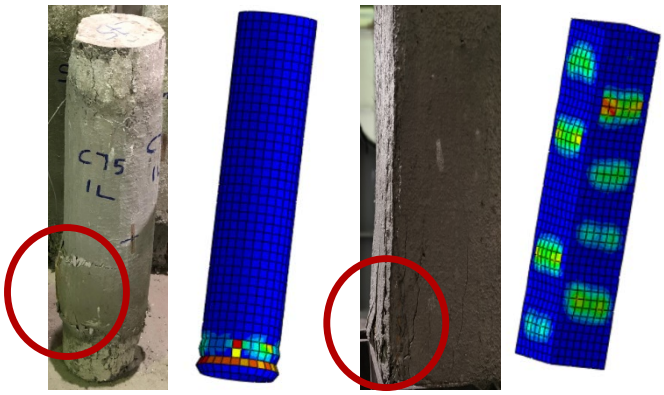

(b)

Figure 10: Comparison of failure modes: FEM vs Tello et al. [31] (a) control specimens (b) strengthened specimens.

The damage location obtained from FEM is consistent with the experimental program as shown in Figure 10. This further verifies that the developed FE model is capable of accurately predicting the behaviour of the strengthened columns both square and circular cross sections. Results from literature and finite element model comparison are presented in Table 4.

3.3. Design Codes

3.3.1. Capacity computation. Although the idea of externally bonded FRP reinforcement for structural strengthening is relatively recent, numerous codes amongst ACI 549.4R-13 [27] have developed and published a detailed guideline for the design and construction of externally bonded FRP-RC structures, however most of these provisions are very conservative. Comparison is drawn on the basis of column axial capacity between the ACI 549.4R-13 provisions and results from the finite element analysis. Specifically, the following equations are utilized:

$$P_n = 0.85[0.85f'_c(A_g - A_{st}) + f_y A_{st}] \quad (spiral) \tag{12}$$

$$P_n = 0.8[0.85f'_c(A_g - A_{st}) + f_y A_{st}] \quad (ties) \tag{13}$$

$$\varepsilon_{ccu} = \varepsilon'_c\left(1.50 + 12k_b\frac{f_l}{f'_c}\left(\frac{\varepsilon_{fe}}{\varepsilon'_c}\right)^{0.45}\right) \tag{14}$$

$$P_n = 0.85[0.85f'_{cc}(A_g - A_{st}) + f_y A_{st} \quad (spiral) \tag{15}$$

$$P_n = 0.8[0.85f'_{cc}(A_g - A_{st}) + f_y A_{st} \quad (ties) \tag{16}$$

where:

P_n *is the nominal axial strength*

A_g *is the gross cross sectional area*

A_e *is the effective confined area*

A_c *is the net cross sectional area*

A_{st} *is the area of longitudinal steel*

A_f *is the mesh per unit width area*

b and h are the short and long dimensions on a rectangular section

D is the diameter of a circular section

r_c *is the radius of the edges on a rectangular section*

ρ_g *is the ratio of longutudinal steel to cross sectional area*

f_y *is the tensile yield strength of steel*

f'_c *is the compressive strength*

f'_{cc} *is the axial confined concrete compressive strength*

$\psi_f = 0.95$ *(strength reduction factor based on committee's judgement)*

κ_a *is the FRCM reinforcement efficiency factor*

f_1 *is the confinement pressure due to FRCM strengthening*

n *is the number of layers of mesh in FRCM*

E_f is the tensile modulus of elasticity of FRCM

ε_{ccu} is the ultimate confined concrete axial compressive strain (from FEA)

ε_{fe} is the effective strain level in the FRCM at failure

k_b is the efficiency factor

ε'_c is the strain corresponding to f'_c

f'_{c0} is the compressive strength of the unconfined concrete ($0.85f'_c$)

ε_{cu} is the ultimate strain in the unconfined concrete (0.003)

3.3.2. Safety factor. ACI 549.4R-13 [27] design guideline for externally bonded FRP suggests that the design strength should be determined using a reduction factor only for FRP ranging between 0.5-0.95 depending on the type of FRP and environmental condition. ACI 549.4R-13 [27] also recommends a strength reduction factor of 0.65 for tied columns and 0.75. for spiral columns in addition to the material safety factor. An additional strength reduction factor of 0.85 is applied to the contribution of FRP reinforcement to the axial capacity.

3.3.3. Allowable strain. ACI 318-14 [34] prescribes 0.003 as allowable strain of concrete.

3.4. Axial Ductility

Axial ductility in this study is defined as the ratio of the axial deformation of the column specimen on the descending part of the axial capacity versus deformation plot to the axial deformation on the ascending part taken at 85% of the axial capacity. Axial ductility is given by equation 17 below and illustrated in Figure 11.

$$\eta - \text{axial} = \frac{\Delta_{0.85-post}}{\Delta_{0.85-prior}} \tag{17}$$

where:

$\Delta_{0.85-prior} = axial\ deformation\ at\ 0.85 * Pu\ prior\ to\ ultimate\ load\ (mm)$

$\Delta_{0.85-post} = axial\ deformation\ at\ 0.85 * Pu\ post\ ultimate\ load\ (mm)$

$\eta - axial =\ axial\ ductility\ (unitless)$

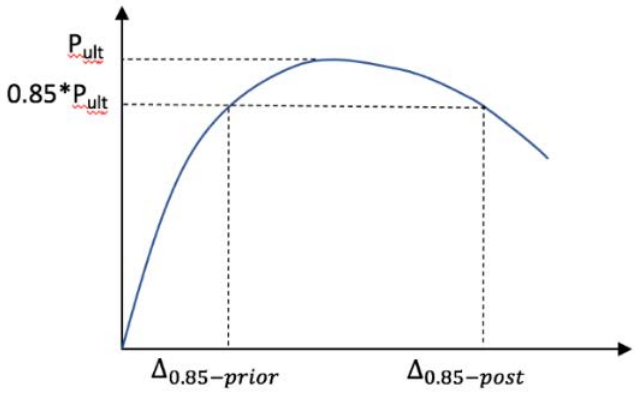

Figure 11: Illustration of Axial Ductility Computation

Chapter 4. Parametric Study

In this section the test matrix along with the different parameters investigated, specimen dimensions, concrete grade, and reinforcement detailing are discussed in detail. A total 180 cases of FE models are developed to investigate the behaviour of FRCM retrofitted RC columns using a concrete compressive strength of 30 MPa and a fixed longitudinal reinforcement ratio of 0.02 typical to columns. The parameters investigated include: (a) cross section type (square vs circular), (b) FRCM layers (1, 2, 3, 4 layers), (c) damage level (mild, moderate and severe damage), (d) eccentricity ratio (0.0, 0.3, 0.5, 0.75, 1.0, 1.25 and 1.5), (e) column type (short vs slender). The specimens have square and circular cross sections of 150mm sides and 170mm diameter respectively with tie and hoop spacing of 75mm. The short and slender columns are limited to a length of 800mm and 1200mm to ensure short and slender column behaviour respectively according to ACI 318 [34] guidelines. Figure 12 below presents the specimen geometry and detailing. Concentric static loading is applied on the short columns while eccentric static loading is applied to the slender columns to study the confinement behaviour of FRCM retrofitted RC columns. Displacement controlled loading condition is used and material nonlinearities in concrete, cement mortar and composite are incorporated in the FE model. The test matrix is divided into two main groups, Series I for short concentrically loaded columns and Series II for slender eccentrically loaded specimens.

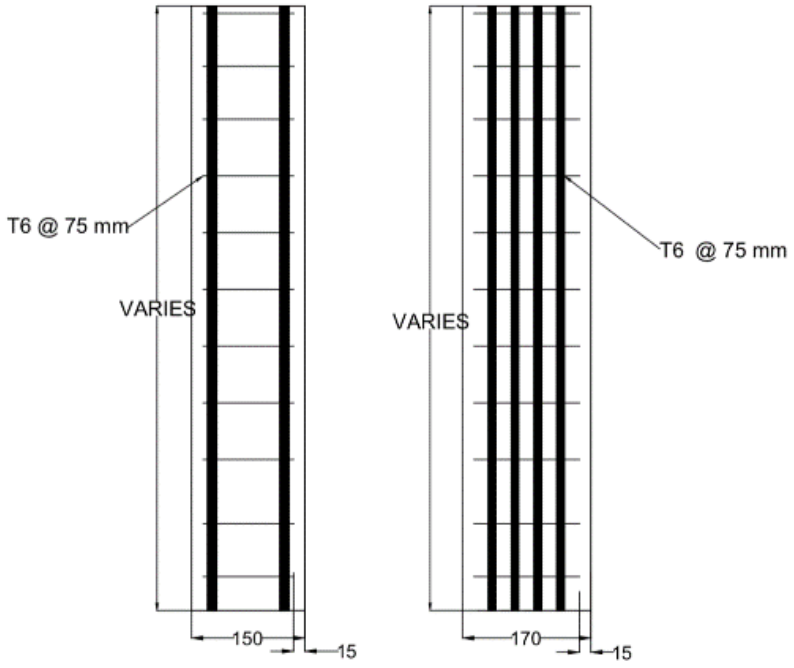

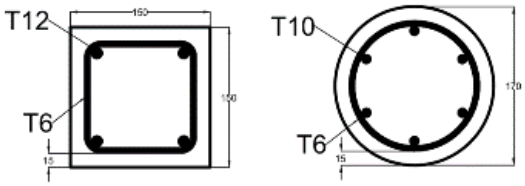

Figure 12: Square and Circular Specimen Sections and Details

Series I is composed of 40 short columns with zero eccentricity ratio, i.e., e/h= 0.0 where 'e' is the applied eccentricity (mm) and h is the width/diameter of the specimen cross section (mm). This group is divided into two groups of 20 square and 20 circular columns designated with prefixes S and C, respectively. Each group of 20 columns is further subdivided into four groups of 5 columns with varying pre-damage level in terms of percentage loss in steel yield stress viz: 0%, 30%, 50% and 70% representing undamaged, mild, moderate, and severely damaged columns, respectively. Each group of 5 columns contains 4 specimens strengthened with 1, 2, 3 and 4 layers of PBO-FRCM and 1 control specimen with no PBO-FRCM to serve as a benchmark to measure the performance of the strengthened specimens. Table 5 and Figure 13 below show the text matrix and naming scheme of Series I.

Table 5: Test Matrix Series I

FRCM Ply	Pre-damage Level (% loss in yield stress)	Cross Section
0L, 1L, 2L, 3L, 4L	0%, 30%, 50%, 70% Control, Mild, Moderate, Severe	Square, Circular

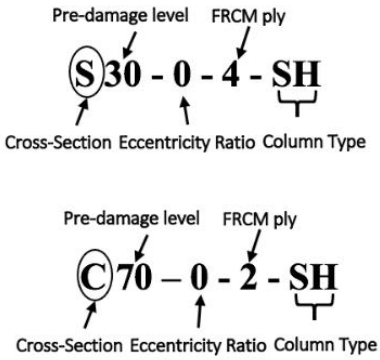

Figure 13: Series I Specimen Identification

Series II is composed of 140 slender columns with eccentricity ratio, e/h ranging from 0.0 to 1.5 where 'e' is the applied eccentricity (mm) and h is the diameter of the specimen cross section (mm). All columns in this group are circular and denoted with a prefix C. The group is subdivided into four groups of 35 columns with varying pre-damage level in terms of percentage loss in steel yield stress: 0%, 30%, 50% and 70% representing control, mild, moderate, and severely damaged columns respectively. Each group of 35 columns is further divided into 5 groups containing 7 columns for each eccentricity ratio, e/h= 0.0, 0.3, 0.5, 0.75, 1.0, 1.25 and 1.5. Each group of 5 columns contained: four specimens strengthened with 1, 2, 3 and 4 layers of PBO-FRCM and one control specimen with no PBO-FRCM to serve as a benchmark to measure the performance of the strengthened specimens. Table 6 and Figure 14 below show a summary of the text matrix and naming scheme of Series II.

Table 6: Test Matrix Series II

FRCM Ply	Eccentricity Ratio	Pre-damage Level (% loss in yield stress)
0L, 1L, 2L, 3L, 4L	0.0, 0.3, 0.5, 0.75, 1.0, 1.25, 1.5	0%, 30%, 50%, 70% Control, Mild, Moderate, Severe

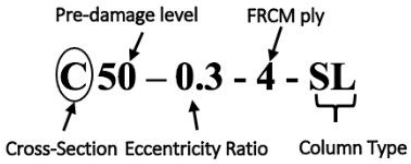

Figure 14: Series II Specimen Identification

The variation of the layers of FRCM is modelled using the confined compressive strengths from ACI 549.4R-13 [27] equations mentioned in section 3.1.3 of this proposal and the results of the variation are reported in Tables 7 and 8.

Chapter 5. Results and Analysis

This section presents summary of the results and discussion reported in terms of load and corresponding strains plots, column axial capacity bar charts and trend plots.

5.1. Series I – Concentrically Loaded

Tables 7 and 8 present a results summary of ultimate axial load (Pu) and corresponding axial ductility (η) and the observed modes of failure in each specimen. The axial ductility η-axial given by equation 17 are also reported.

Table 7: Result Summary & Failure Modes (Square)

Column ID	Axial Capacity Pu (kN)	Increase in Pu (%)	Axial Ductility η-axial	Increase in η-axial (%)	Failure Mode
S0-0-0-SH	819	Control	1.66	Control	Concrete Crushing
S0-0-1-SH	893	9	1.86	12	Matrix Damage
S0-0-2-SH	952	16	1.93	17	Matrix Damage
S0-0-3-SH	966	18	2.00	20	Matrix Damage
S0-0-4-SH	981	20	2.09	26	Matrix Damage
S30-0-0-SH	816	0	1.59	-4	Concrete Crushing
S30-0-1-SH	844	3	2.05	24	Matrix Damage
S30-0-2-SH	902	10	2.19	32	Matrix Damage
S30-0-3-SH	916	12	2.13	28	Matrix Damage
S30-0-4-SH	931	14	2.23	34	Matrix Damage
S50-0-0-SH	772	-6	1.68	1	Concrete Crushing
S50-0-1-SH	799	-2	2.20	33	Matrix Damage
S50-0-2-SH	858	5	2.35	42	Matrix Damage
S50-0-3-SH	872	6	2.23	35	Matrix Damage
S50-0-4-SH	887	8	2.26	37	Matrix Damage
S70-0-0-SH	724	-12	1.77	7	Concrete Crushing
S70-0-1-SH	754	-8	2.30	39	Matrix Damage
S70-0-2-SH	809	-1	2.16	30	Matrix Damage
S70-0-3-SH	821	0	2.13	28	Matrix Damage
S70-0-4-SH	836	2	2.17	31	Matrix Damage

Table 8: Result Summary & Failure Modes (Circular)

Column ID	Axial Capacity Pu (kN)	Increase in Pu (%)	Axial Ductility η-axial	Increase in η-axial (%)	Failure Mode
C0-0-0-SH	878	Control	1.56	Control	Concrete Crushing
C0-0-1-SH	1046	19	3.41	119	Matrix Damage
C0-0-2-SH	1085	24	3.68	136	Matrix Damage
C0-0-3-SH	1141	30	4.03	159	Matrix Damage
C0-0-4-SH	1189	35	3.62	132	Matrix Damage
C30-0-0-SH	885	1	1.56	0	Concrete Crushing
C30-0-1-SH	985	12	3.57	129	Matrix Damage
C30-0-2-SH	1024	17	3.95	154	Matrix Damage
C30-0-3-SH	1080	23	3.94	153	Matrix Damage
C30-0-4-SH	1128	29	3.77	142	Matrix Damage
C50-0-0-SH	839	-4	1.57	1	Concrete Crushing
C50-0-1-SH	929	6	3.28	110	Matrix Damage
C50-0-2-SH	967	10	3.87	148	Matrix Damage
C50-0-3-SH	1018	16	3.85	147	Matrix Damage
C50-0-4-SH	1065	21	3.66	135	Matrix Damage
C70-0-0-SH	789	-10	1.58	1	Concrete Crushing
C70-0-1-SH	856	-3	3.36	115	Matrix Damage
C70-0-2-SH	896	2	4.12	164	Matrix Damage
C70-0-3-SH	949	8	4.01	157	Matrix Damage
C70-0-4-SH	997	14	3.36	115	Matrix Damage

5.1.1. Axial capacity and ductility enhancement. Significant enhancements were observed in axial capacity and ductility as presented in Tables 7 and 8. Specimens (S0-0-0-SH and C0-0-0-SH) are used as benchmark for comparison to measure performance and the ability of the PBO-FRCM strengthening system to restore the original capacity of the damaged specimens. These two specimens will henceforth be referred to as control specimens for square and circular specimens of Series I, respectively. For the undamaged specimens strengthened with 1, 2, 3 and 4 FRCM

layers, increase in axial capacity of 9%, 16%, 18% and 20%, with axial ductility increase of 12%, 17%, 20% and 26% was observed for square specimens (S0-0-1-SH, S0-0-2-SH, S0-0-3-SH and S0-0-4-SH) respectively when compared to the corresponding control specimen (S0-0-0-SH), while axial capacity increase of 19%, 24%, 30% and 35%, with increase in axial ductility of 119%, 136%, 159% and 132% for circular specimens (C0-0-1-SH, C0-0-2-SH, C0-0-3-SH and C0-0-4-SH) respectively was observed when compared to the control specimen (C0-0-0-SH). These enhancement effects are visible in Figure 15.

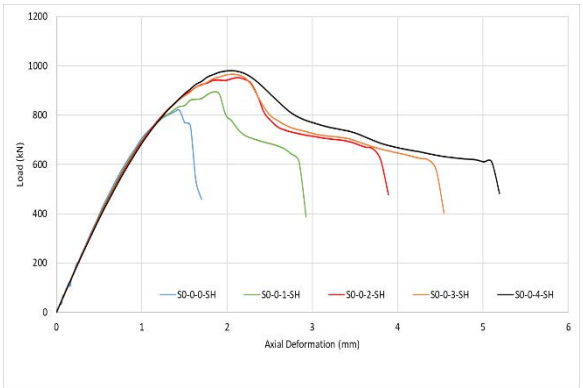

(a)

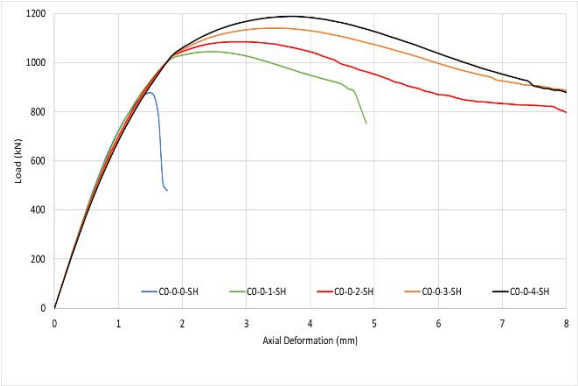

(b)

Figure 15: Load versus Axial Deformation Plot (No Damage) (a) square (b) circular

Similarly, for mildly damaged specimens strengthened with with 1, 2, 3 and 4 FRCM layers, increase in axial capacity of 3%, 10%, 12% and 14%, with axial ductility increase of 24%, 32%, 28% and 34% was observed for square specimens (S30-0-1-SH, S30-0-2-SH, S30-0-3-SH and S30-0-4-SH) respectively when compared to the corresponding control specimen (S0-0-0-SH), while axial capacity increase 12%, 17%, 23% and 29%, with increase in axial ductility of 129%, 154%, 153% and 142% for circular specimens (C30-0-1-SH, C30-0-2-SH, C30-0-3-SH and C30-0-4-SH)

respectively was observed when compared to the control specimen (C0-0-0-SH). These enhancement effects are visible in Figure 16.

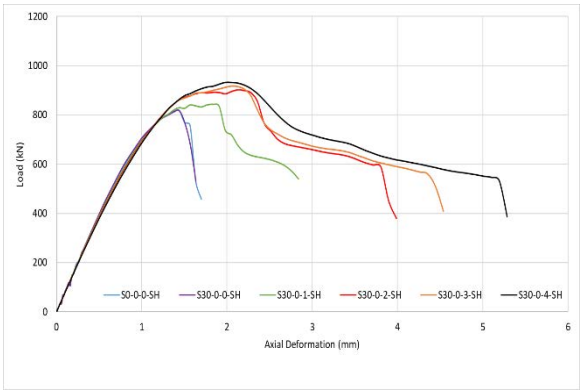

(a)

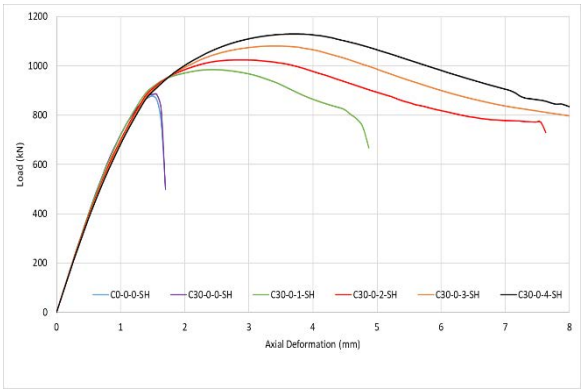

(b)

Figure 16: Load versus Axial Deformation Plot (Mild Damage) (a) square (b) circular

Likewise, for moderately damaged specimens strengthened with 1, 2, 3 and 4 FRCM layers, decrease in axial capacity of 2% and increase of 5%, 6% and 8%, with axial ductility increase of 33%, 42%, 35% and 37% was observed for square specimens (S50-0-1-SH, S50-0-2-SH, S50-0-3-SH and S50-0-4-SH) respectively when compared to the corresponding control specimen (S0-0-0-SH), while axial capacity increase 6%, 10%, 16% and 21%, with increase in axial ductility of 110%, 148%, 147% and 135% for circular specimens (C50-0-1-SH, C50-0-2-SH, C50-0-3-SH and C50-0-4-SH) respectively was observed when compared to the control specimen (C0-0-0-SH). Figure 17 shows a visual of the enhancement effects.

For severely damaged specimens strengthened with 1, 2, 3 and 4 FRCM layers, decrease in axial capacity of 8% and 1%, and increase in axial capacity of 0% and 2%, with axial ductility increase of 39%, 30%, 28% and 31% was observed for square specimens (S70-0-1-SH, S70-0-2-SH, S70-0-3-SH and S70-0-4-SH) respectively when

compared to the corresponding control specimen (S0-0-0-SH), while axial capacity decrease of 3% and axial capacity increase of 2%, 8% and 14%, with increase in axial ductility of 115%, 164%, 157% and 115% for circular specimens (C70-0-1-SH, C70-0-2-SH, C70-0-3-SH and C70-0-4-SH) respectively was observed when compared to the control specimen (C0-0-0-SH). These effects are shown in Figure 18.

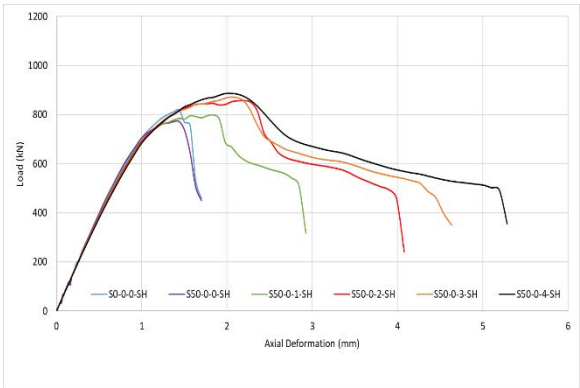

(a)

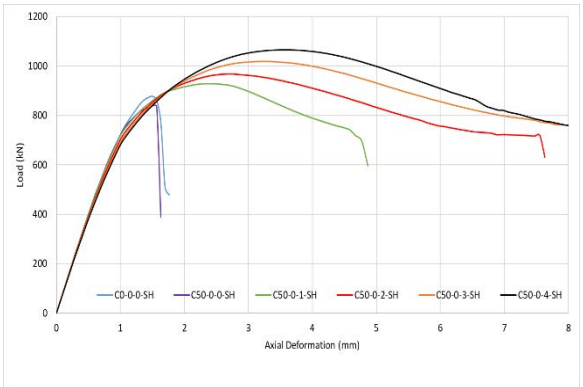

(b)

Figure 17: Load versus Axial Deformation Plot (Moderate Damage) (a) square (b) circular

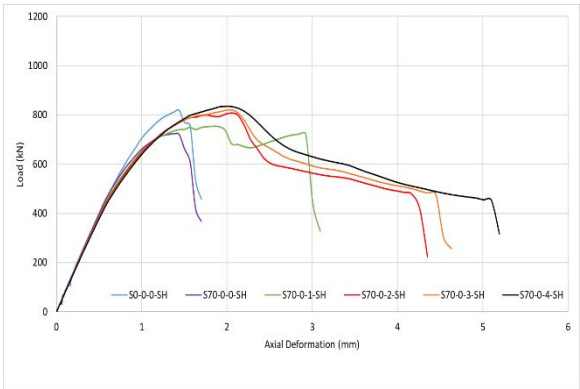

(a)

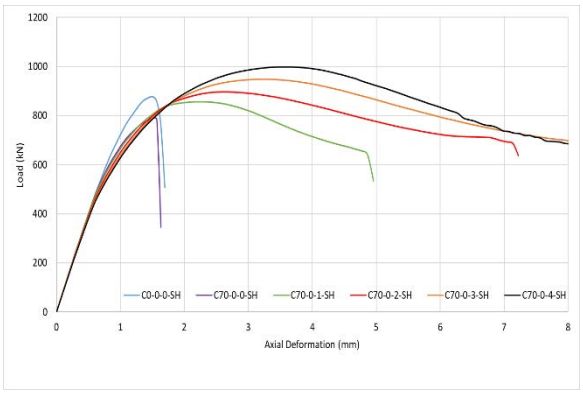

(b)

Figure 18: Load versus Axial Deformation Plot (Severe Damage) (a) square (b) circular

5.1.2. Effect of PBO-FRCM layers. From Figures 15-18, it is visible that enhancement in the axial load capacity and ductility is correlated with increase in number FRCM layers. In summary, for the mildly damaged specimens, 1 layer of FRCM is required to restore the original capacity of the control specimen for both square and circular specimens with axial capacity enhancement of 5% and 6% respectively, however 4 layers are required to achieve optimal ductility enhancement of 34% in the square specimen and 2 layers are required for optimal ductility of 154% for circular specimen.

For the moderately damaged specimens, 2 layers of FRCM are required to restore the original capacity of the control specimen for square cross section and 1 layer for circular cross section with axial capacity enhancement of 5% and 6% respectively, whilst 2 layers yield optimal ductility enhancement of 42% and 148% in both the square and circular specimens, respectively.

For the severely damaged specimens, 3 layers of FRCM are required to restore the original capacity of the control specimen for square cross section and 2 layers are required for circular cross section with axial capacity enhancement of 0% and 2% respectively, whilst 4 layers are required for optimal ductility enhancement of 31% for square specimen and 2 layers yield optimal ductility enhancement of 164% for the circular specimen. These finding are summarized in Figures 19-20.

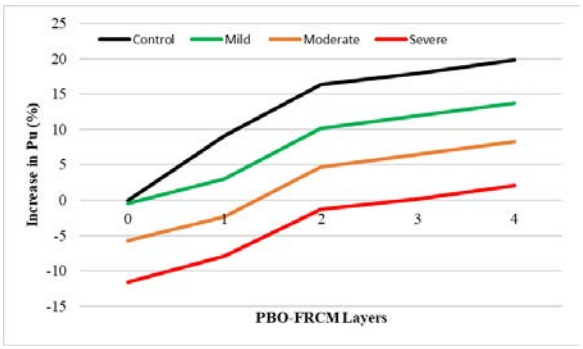

(a)

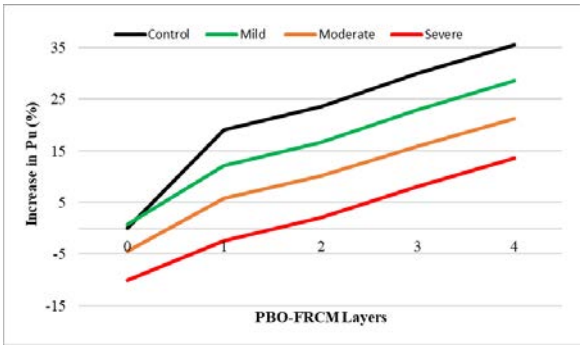

(b)

Figure 19: Axial Capacity Enhancement vs FRCM Layers (a) square (b) circular

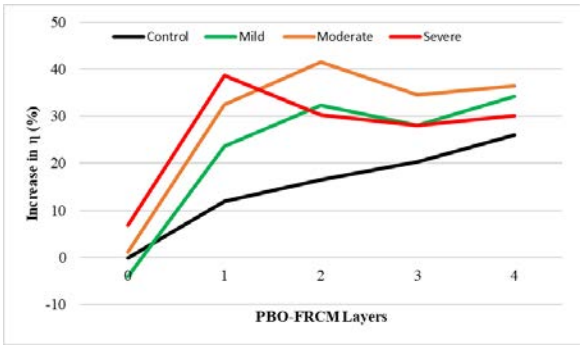

(a)

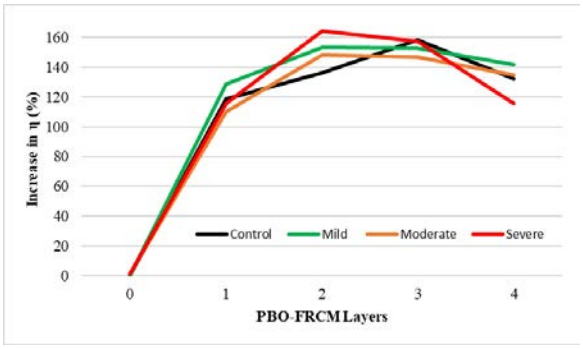

(b)

Figure 20: Axial Ductility Enhancement vs FRCM Layers (a) square (b) circular

5.1.3. Effect of cross-section. From Tables 7-8 and Figures 15-18, it is evident that the axial capacity and ductility enhancement in the circular specimens is significantly higher than the corresponding square specimens. This difference is attributed to the confinement models used in developing the finite element models which considers the effective confinement phenomenon discussed in section 3.1.3 of this study and is consistent with the findings in published literature [22], [28], [30] and [33].

The difference in axial capacity between the square and circular cross sections is significant despite the similarity in reinforcement ratio and configuration. The confinement deficit in square columns can be reduced by chamfering or rounding the corners of the square cross sectional columns before strengthening in order to reduce stress concentrations in the corners of the column resulting in uneven stress distribution to the FRCM composite. This approach is very common in most strengthening applications.

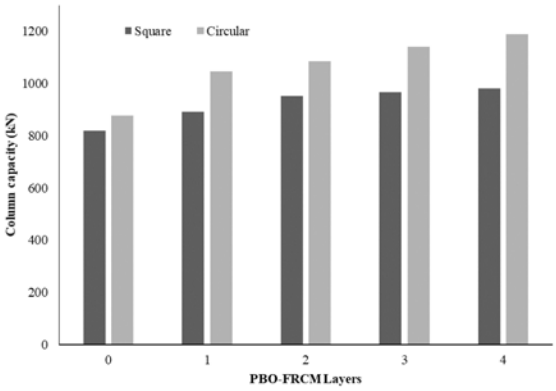

(a)

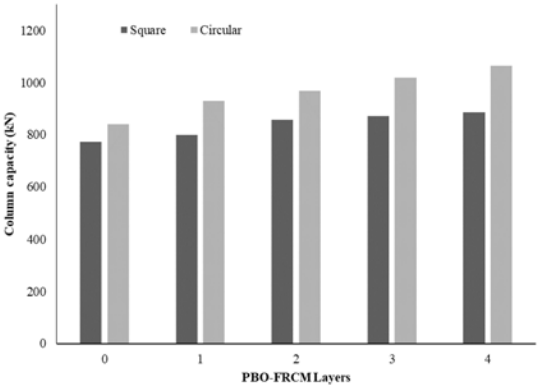

(b)

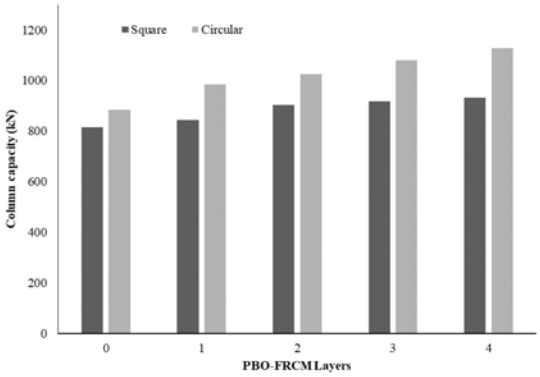

(c)

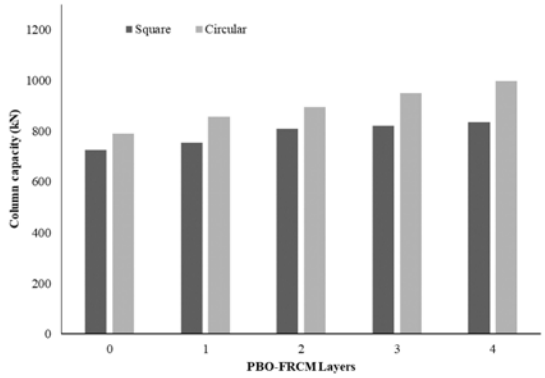

(d)

Figure 21: Axial Capacity Comparison: Square vs Circular (a) Control (b) Mild (c) Moderate (d) Severe

An average difference in axial capacity and ductility of 13% and 35% was observed purely attributed to shape factor. Figure 21 below show enhancement differences between square and circular specimens due to the cross-sectional effect.

5.1.4. Effect of damage level. The increase in axial capacity is less prominent as damage severity in the specimens increases. Maximum axial capacity increase of 20%,14%, 8% and 2% is observed in square specimens while 35%, 29%, 21% and 14% was observed in circular specimens for undamaged, mild, moderate, and severely damaged groups, respectively.

Figure 22 shows the strength increase at different damage levels for square and circular cross sections. A clear positive trend is observed between increase in axial capacity and increase in number of FRCM layers.

Figure 23 shows the strength increase at different damage levels for square and circular cross sections of all the specimens in the study group. Higher axial capacity is

observed in every group for the circular cross section column. The difference diminishes as the level of corrosion damage gets severe

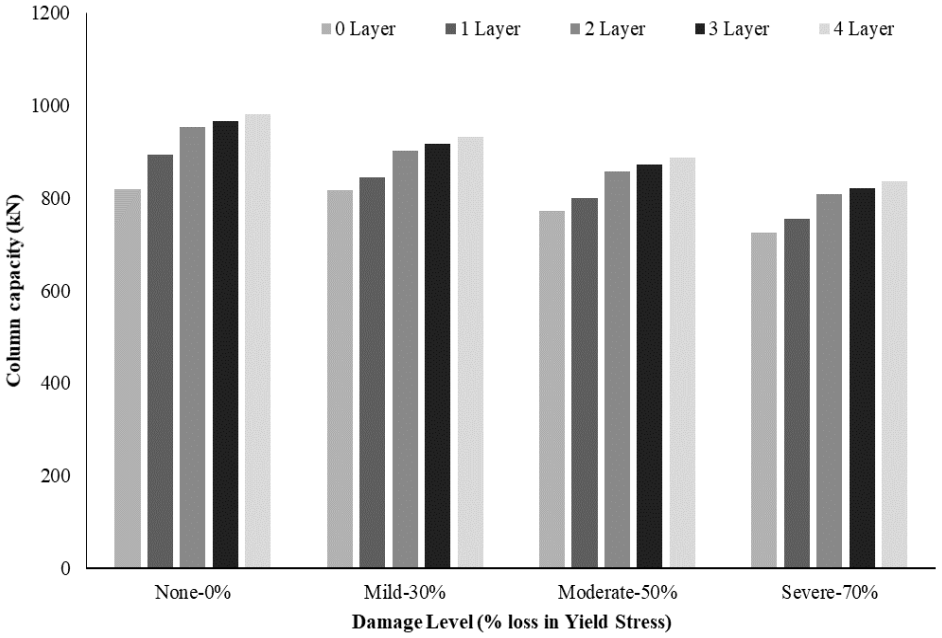

(a)

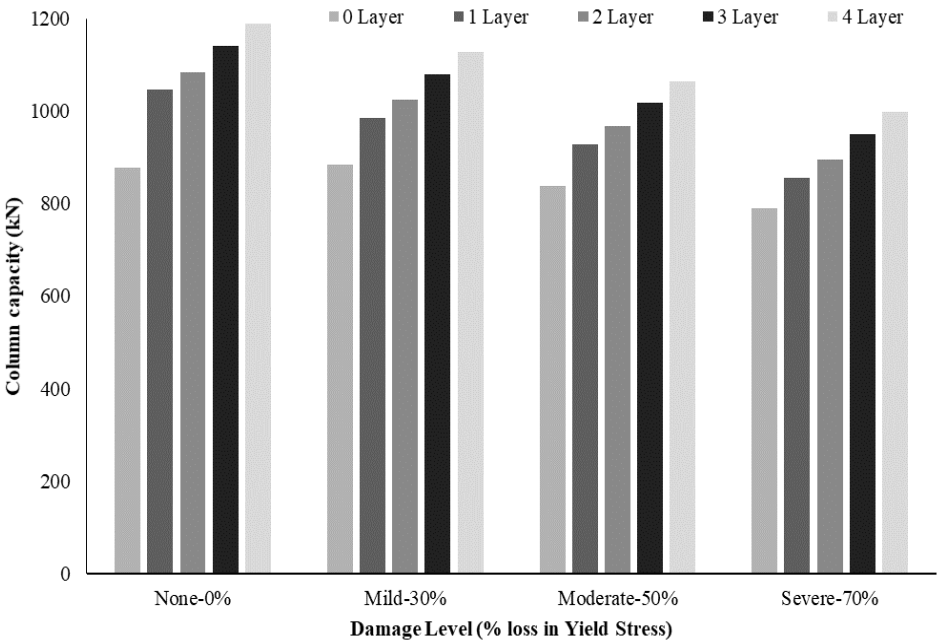

(b)

Figure 22: Effect of Damage level on Axial Capacity (a) square (b) circular

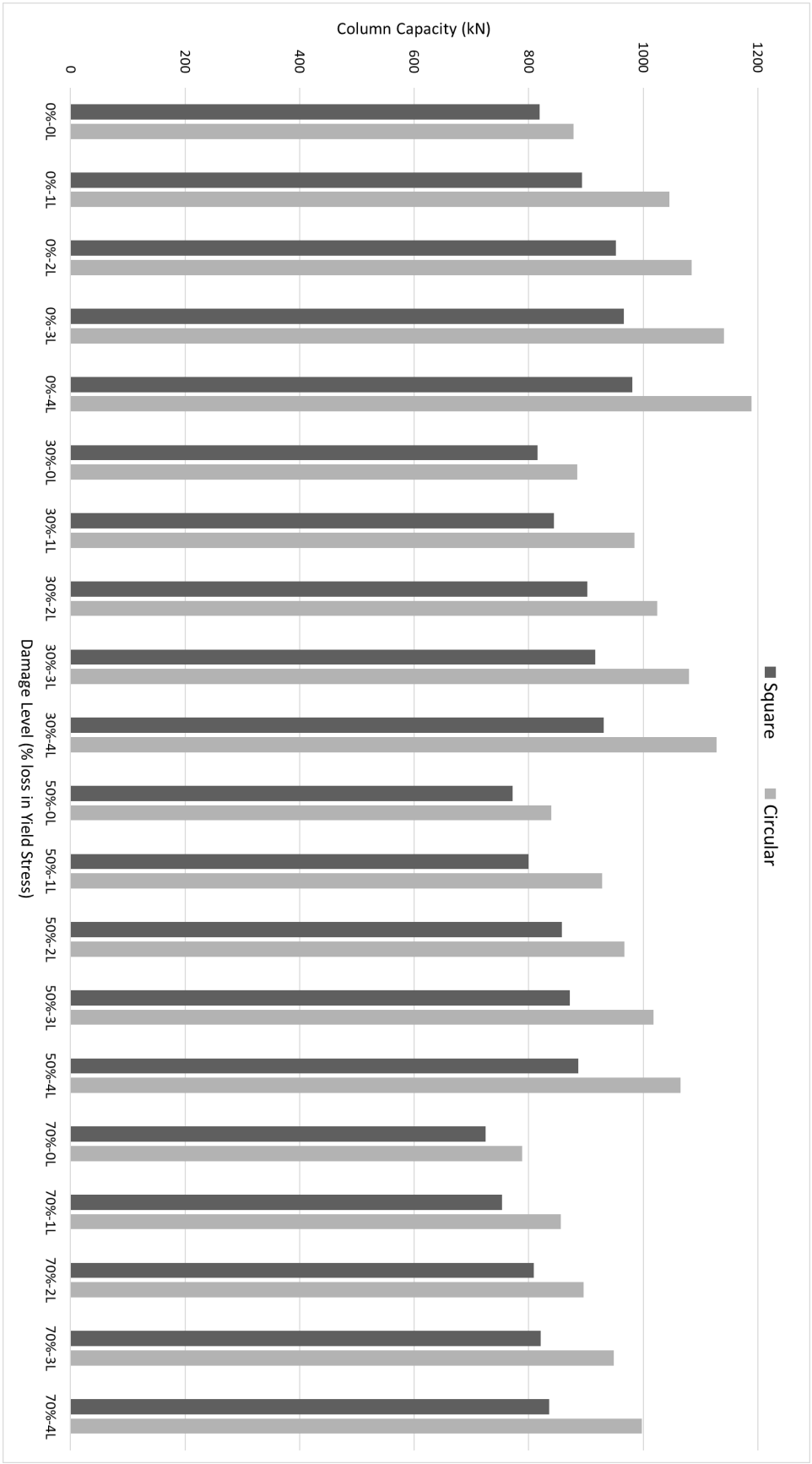

Figure 23: Effect of Damage level on Axial Capacity (square vs circular)

5.1.5. Failure modes. Two distinct failure modes were observed in the models: concrete crushing and matrix damage. Yielding in longitudinal reinforcement was achieved during the analysis in all the strengthened specimens. Yielding of the steel reinforcement is confirmed through monitoring the strain levels in the steel reinforcement. Yielding of steel reinforcement in the square specimens occurs earlier and is more severe than the circular specimens as shown in Figure 24 below. This is related to effective confinement that occurs in circular cross sections. This observation is consistent for all FRCM layers and across all damage levels.

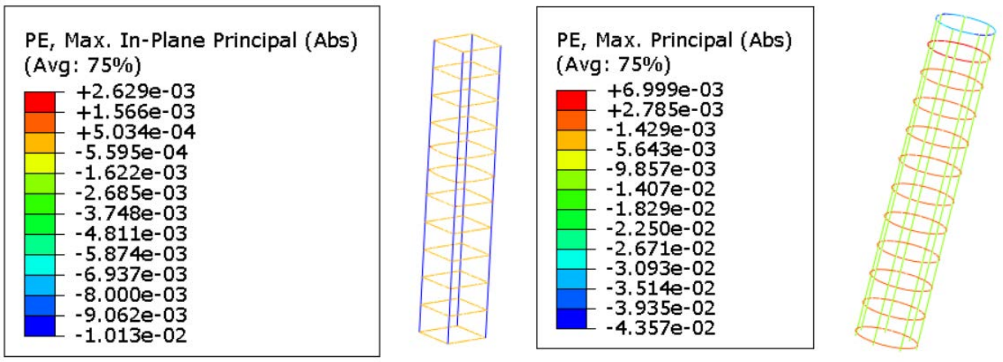

(a) (b)

Figure 24: Yielding in Transverse and Longitudinal Reinforcing Steel (a) Square Specimens (b) Circular Specimens

Concrete crushing is delayed by the confinement pressure from the FRP in all the strengthened specimens and consequently the failure mode observed in the strengthened specimens is matrix damage which is indicated by the sudden drop in the axial load micro-strain plots presented in Figures 15-18. This drop occurs at lower strain levels and is more sudden in the square specimens compared to their circular counterparts indicating a more ductile behaviour and failure mode in the circular specimens. The cementitious mortar was completely damaged axially upon initial loading in all the specimens which means that the mortar did not contribute to the axial capacity of the columns as modelled. Wrinkling was observed in the FRCM due to axial shortening of the column however, delamination of FRCM was not observed in any of the specimens. This is a reasonable observation as delamination can be prevented by splicing the FRP and alternating the splice location of subsequent layers. Failure modes of each specimen are reported in Tables 7 and 8. The control (unstrengtened) specimens failed by concrete crushing while all the strengthened specimens failed by matrix

damage in both square and circular specimens. Figures 25 shows the compressive damage in unstrengtened and strengthened specimens.

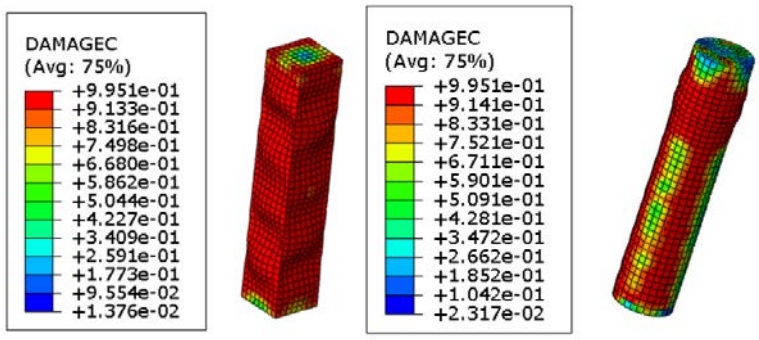

(a)

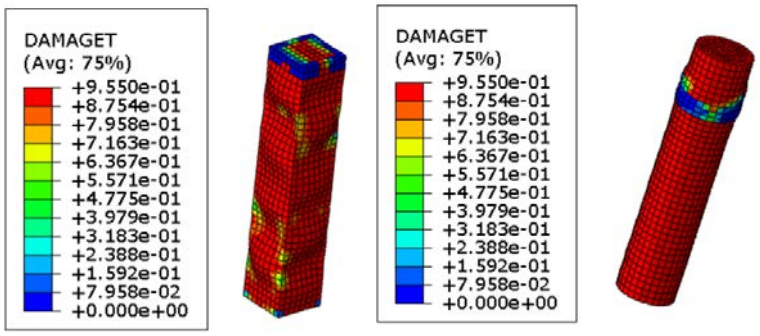

(b)

Figure 25: Concrete Damage (a) Compressive Damage (Square and Circular Specimens) (b) Tensile Damage (Square and Circular Specimens)

Figure 26(a) shows the stress concentration in the corners of the square cross-sectional specimen leading to stress build-up in a small area of the FRCM and a more abrupt failure mode while the stresses are distributed on the FRCM on the circular column allowing the FRP fibers to strain evenly leading to a gentler, more ductile failure mode as evident in the axial capacity strain plots from Figures 15-18.

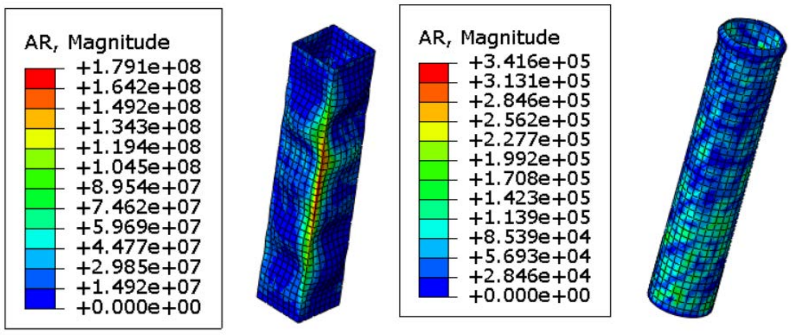

(a) (b)

Figure 26: FRCM Stress Distribution/Concentration (a) Square Specimen (b) Circular Specimen

Figure 26(b) shows bulging on the face of the FRCM between the ties in the square specimen while no bulging is observed on the circular specimen. This is also attributed to uniform stress distribution along the circumference of the circular column due to effective confinement whilst severe stress concentrations result in bulging due to inadequate confinement. Figure 27 show the initial locations FRCM damage in matrix, consistent with the bulging and stress concentration zones in the square specimen and wrinkling zone in the circular specimen.

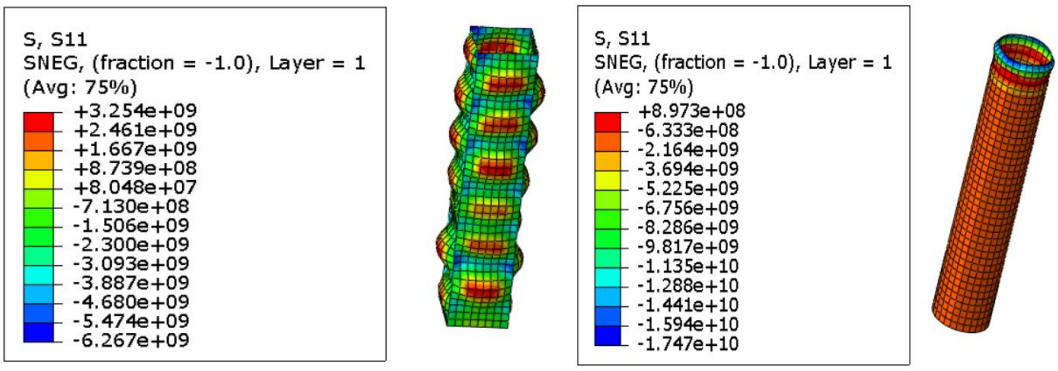

(a) (b)

Figure 27: FRCM Stresses (a) Square Specimen (b) Circular Specimen

5.1.6. Comparison between FE results and analytical predictions. Results obtained from the finite element analyses are compared to analytical predictions prescribed in the ACI 549.4R-13 [27] provisions discussed in section 3.1.3 of this study. Significant under estimation of axial capacity was observed. This is associated with the factors of safety the ACI prescribes to ensure conservative design is achieved. The safety factors include penalizing the contribution of FRP to the column capacity 0.8 and 0.85 for square and circular columns, respectively.

Additionally, introducing a material and environmental safety factor for different FRP fibers, and the prediction of the confinement contribution of the fibers in the f'cc equation. These are exclusive of the minimum eccentricity factor. Difference in axial capacity prediction of up to 19% for square specimens and 22% for circular specimens was observed between the finite element results and the analytical predictions. Tables 9-10 present a detailed summary of the axial capacity obtained from FEM and the axial capacity computed using the ACI 549.4R-13 [27] provisions along with the percentage differences between the two methods for both circular and square columns.

Table 9: Comparison between FEM and analytical predictions (Square)

Column ID	Pu FEM (kN)	Pn Analytical (kN)	% Difference
S0-0-0-SH	819	788	4
S0-0-1-SH	893	801	10
S0-0-2-SH	952	813	15
S0-0-3-SH	966	825	15
S0-0-4-SH	981	837	15
S30-0-0-SH	816	721	12
S30-0-1-SH	844	733	13
S30-0-2-SH	902	745	17
S30-0-3-SH	916	757	17
S30-0-4-SH	931	769	17
S50-0-0-SH	772	675	13
S50-0-1-SH	799	688	14
S50-0-2-SH	858	700	18
S50-0-3-SH	872	712	18
S50-0-4-SH	887	724	18
S70-0-0-SH	724	630	13
S70-0-1-SH	754	642	15
S70-0-2-SH	809	655	19
S70-0-3-SH	821	667	19
S70-0-4-SH	836	679	19

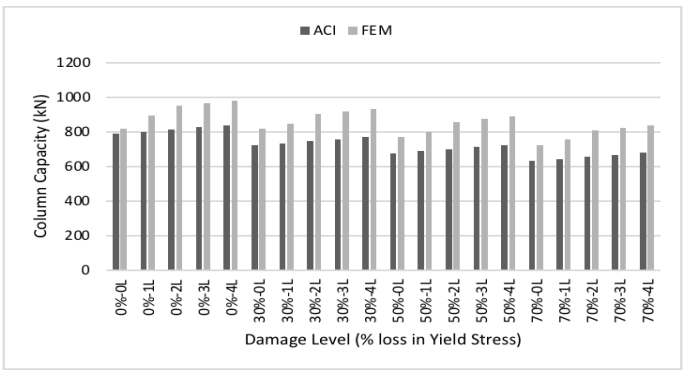

Figure 28: Comparison between FEM and ACI Predictions (Square)

Table 10: Comparison between FEM and analytical predictions (Circular)

Column ID	Pu FEM (kN)	Pn Analytical (kN)	% Difference
C0-0-0-SH	878	802	9
C0-0-1-SH	1046	848	19
C0-0-2-SH	1085	893	18
C0-0-3-SH	1141	939	18
C0-0-4-SH	1189	946	20
C30-0-0-SH	885	731	17
C30-0-1-SH	985	777	21
C30-0-2-SH	1024	822	20
C30-0-3-SH	1080	868	20
C30-0-4-SH	1128	875	22
C50-0-0-SH	839	684	18
C50-0-1-SH	929	730	21
C50-0-2-SH	967	775	20
C50-0-3-SH	1018	821	19
C50-0-4-SH	1065	828	22
C70-0-0-SH	789	637	19
C70-0-1-SH	856	683	20
C70-0-2-SH	896	728	19
C70-0-3-SH	949	774	18
C70-0-4-SH	997	781	22

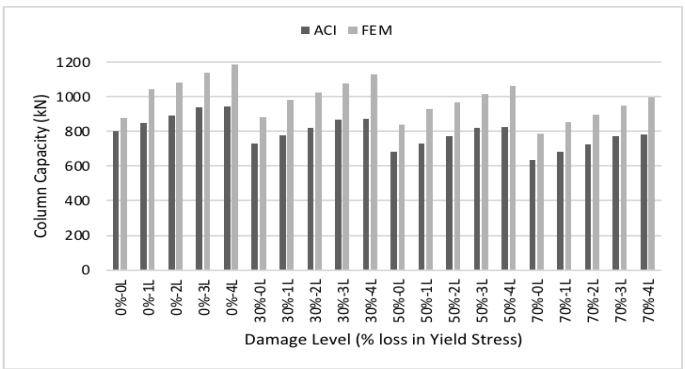

Figure 29: Comparison between FEM and ACI Predictions (Circular)

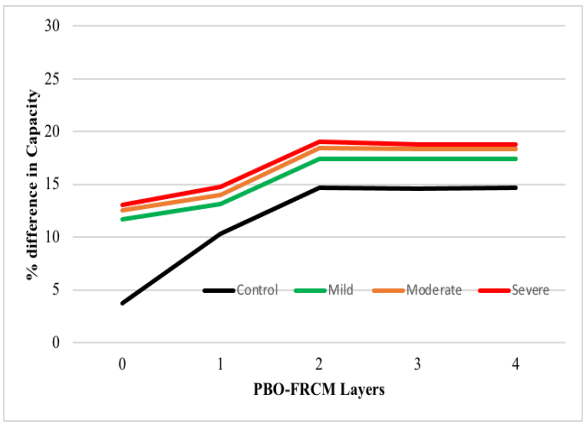

Figure 30: Comparison between FEM and analytical predictions (Square)

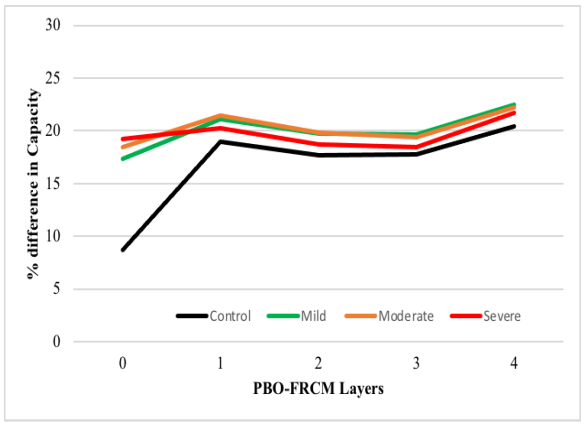

Figure 31: Comparison between FEM and analytical predictions (Circular)

Figures 28-31 show a clear difference between the two approaches of determining the axial capacity of strengthened columns.

5.2. Series I – Eccentrically Loaded

The test results of these specimens further proved that strengthening with PBO-FRCM increased the axial load capacity of all specimens irrespective of damage severity and eccentricity ratio.

5.2.1. Effect of slenderness. An average reduction in axial capacity of 9%, 7%, 6% and 4% in undamaged, mild, moderate, and severely damaged specimens, respectively is observed due to slenderness effect. This reduction is less pronounced with increase in the level of pre-damage. The reduction in capacity gets milder in the strengthened specimens as increase in number of FRCM layers discount the slenderness effect though confinement. Figures 32-33 show the axial capacity loss due to slenderness effect.

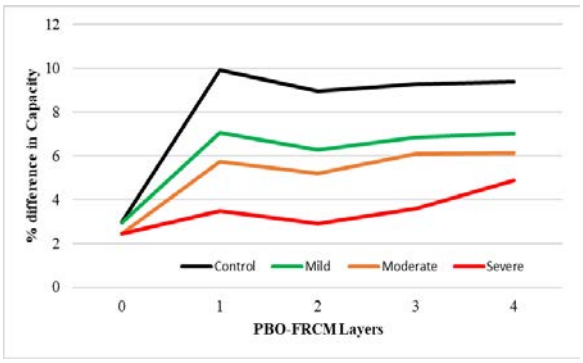

Figure 32: Axial Capacity difference between Slender and Short

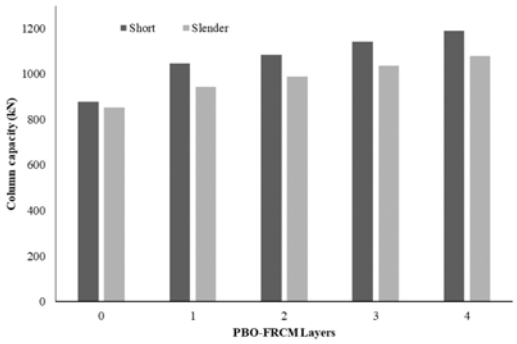

(a)

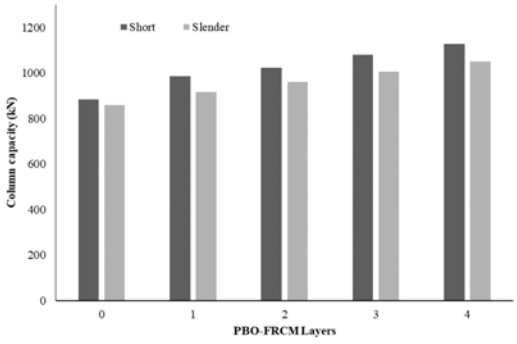

(b)

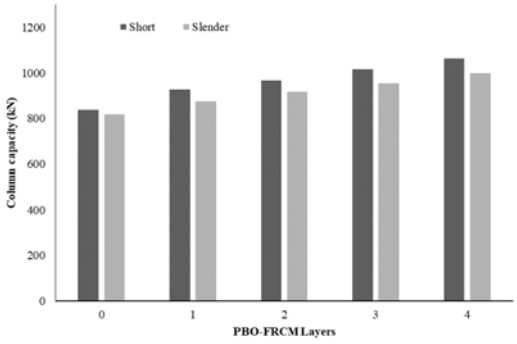

(c)

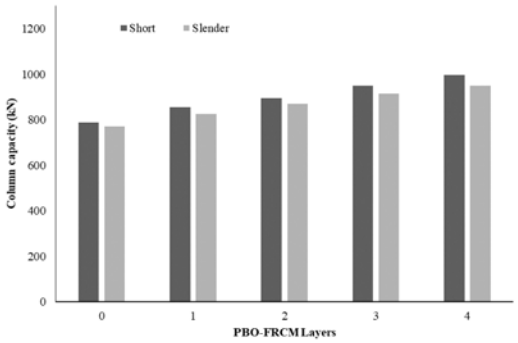

(d)

Figure 33: Axial Capacity Comparison: Short versus Slender (a) Control (b) Mild (c) Moderate (d) Severe

5.2.2. Effect of eccentricity ratio and FRCM layers. The enhancement in the axial load capacity of the specimens increases with increase in number FRCM layers as illustrated in Figure 34. The average enhancement in axial capacity for specimens with low eccentricity ratios (0.3, 0.5, 0.75) and strengthened with 1, 2, 3 and 4 layers of FRCM were 11%, 16%, 21% and 26% respectively, while the average axial capacity enhancement for specimens with medium and large eccentricity ratios (1.0, 1.25, 1.5) and strengthened with 1, 2, 3 and 4 layers of FRCM were 8%, 12%, 17% and 20% respectively, compared with their corresponding unstrengtened control specimens. Figures 34 and 35 show the axial capacity increase resulting from confinement effect from increased FRCM layers.

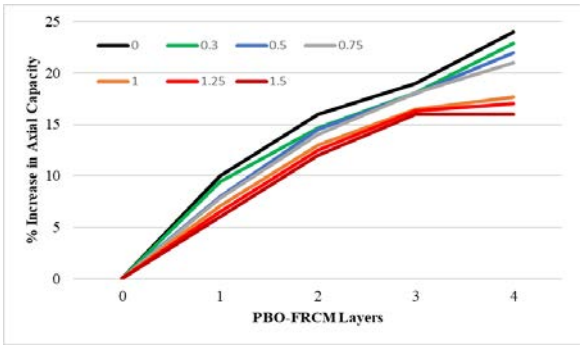

Figure 34: Axial Capacity Enhancement vs FRCM Layers for different Eccentricity ratios

Significant loss in axial capacity is observed as the eccentricity ratio increases, with average axial capacity loss of 16%, 18%, 25%, 29% 33% and 36% for eccentricity ratio values of 0.0, 0.3, 0.5, 0.75, 1.0, 1.25 and 1.5, respectively. The loss in axial capacity due to eccentricity is consistent across the different FRCM layers as shown in Figure 35. It can be noticed that as the eccentricity ratio increases, the amount of axial

capacity loss increases. This observation is consistent for all damage levels visible from Figures 36-37.

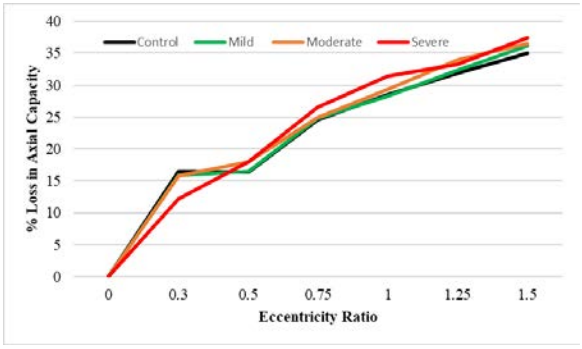

Figure 35: Axial Capacity versus Eccentricity Ratio

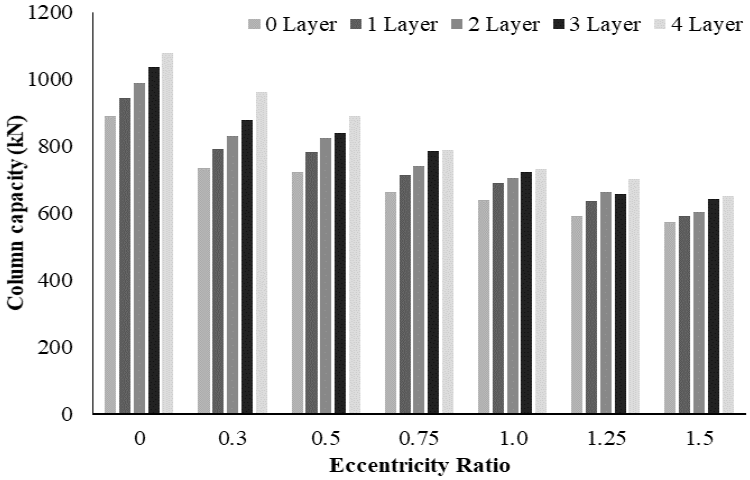

(a)

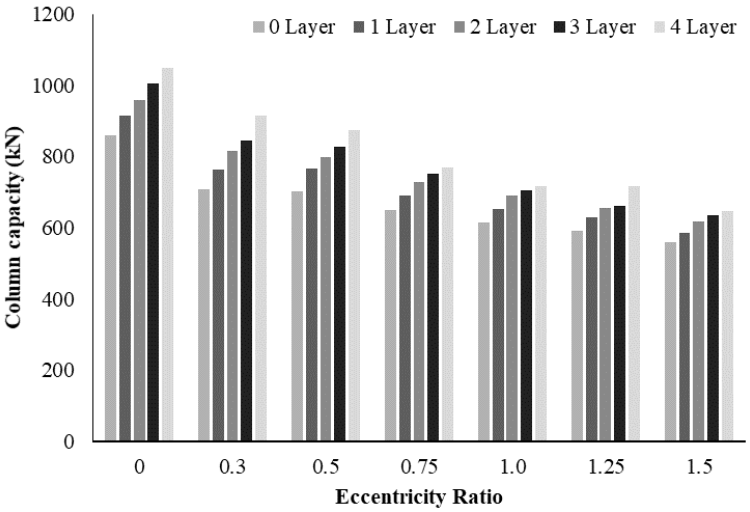

(b)

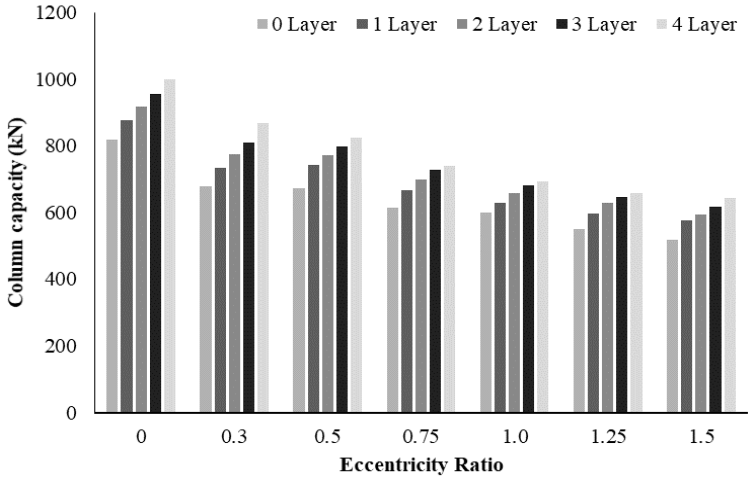

(c)

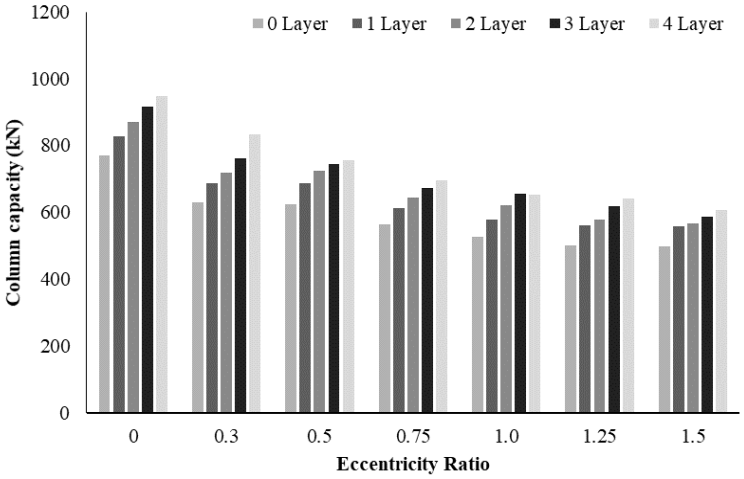

(d)

Figure 36: Axial Capacity Increase with Increase in FRCM Layers vs Eccentricity Ratio (a) Control (b) Mild (c) Moderate (d) Severe

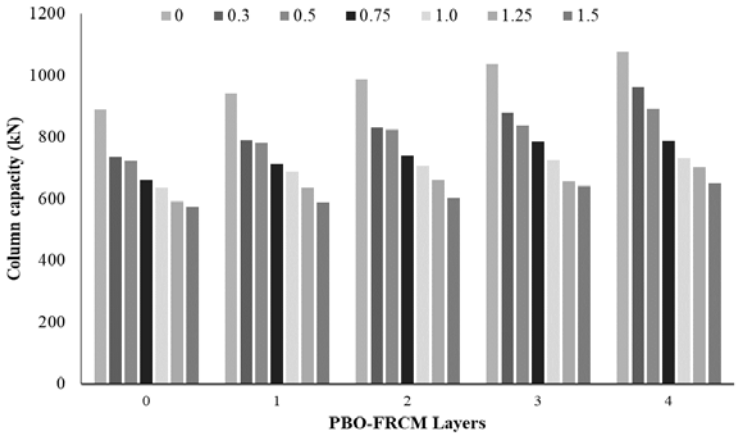

(a)

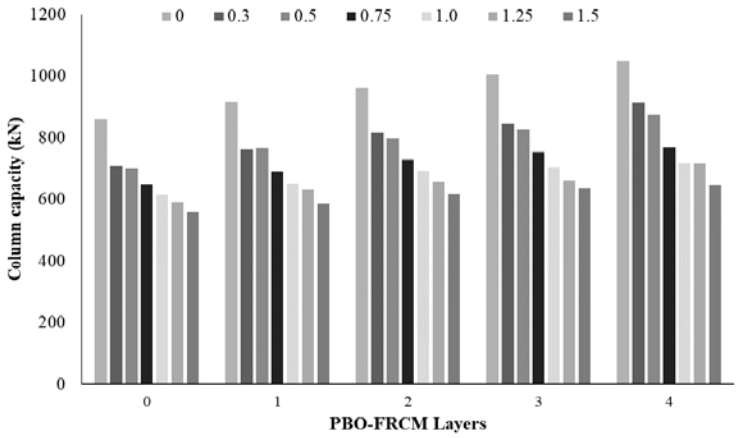

(b)

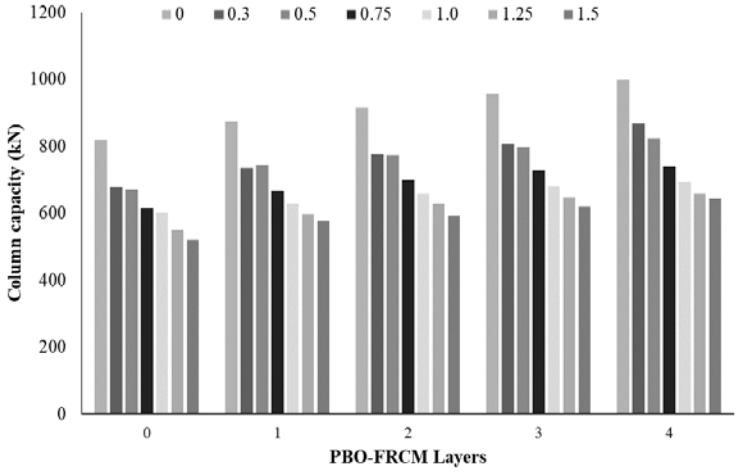

(c)

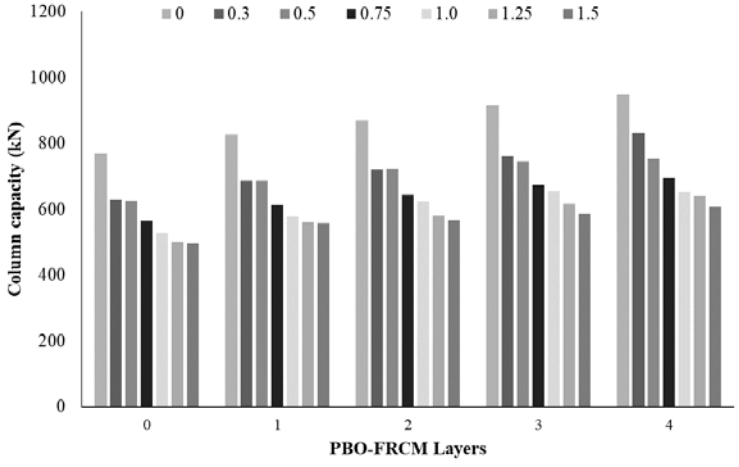

(d)

Figure 37: Axial Capacity Decrease with Increase in Eccentricity Ratio vs FRCM Layers (a) Control (b) Mild (c) Moderate (d) Severe

5.2.3. Effect of damage level. The increase in axial capacity is less prominent as damage severity in the specimens increases. Maximum axial capacity loss of 3%, 8% and 14% is observed for mild moderate and severely damaged specimen respectively compared to the original undamaged specimens. Figure 38 shows the trend of the loss in axial capacity with increase in damage level.

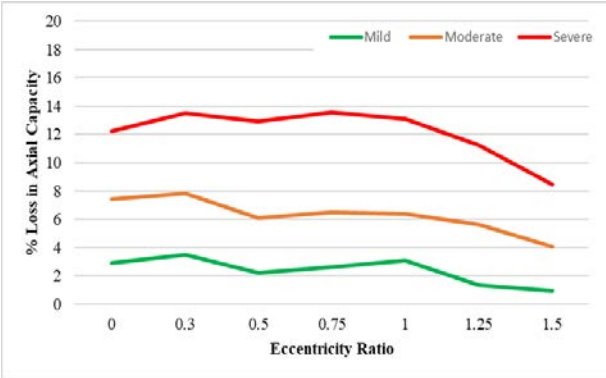

Figure 38: Loss in Axial Capacity at damage levels

5.2.4. Failure modes. The failure modes of the control specimens were characterized by severe concrete crushing that initiated at the middle of the column and propagated towards its ends. The level of propagation and damage to the column increased with increase in eccentricity ratio. The failure of the strengthened specimens was controlled by matrix damage initiated at the top end where the column was loaded. Axial shortening induces wrinkling in the FRCM. Concrete damage in the strengthened specimens follows the same pattern: initiated and the top and bottom ends of the column and propagated towards the middle of the column. Figures 39(a-b) show the concrete damage levels. Slenderness did not affect the mode of failure however the failure of the slender columns occurred and a lower axial load level than the short columns. This failure mode is consistent irrespective of the number of FRCM layers used, however the strengthened specimens exhibited different levels of FRCM damage. The stress in the longitudinal steel bars of all strengthened specimens confirmed that the longitudinal reinforcement yielded during the analysis. The cementitious matrix was completely damaged during the analysis due to extreme axial forces as shown in Figure 39(e), confirming the assumption that the cementitious matrix contributes no axial strength to the specimens. Figure 39(d) shows the wrinkling and damage initiation in FRCM.

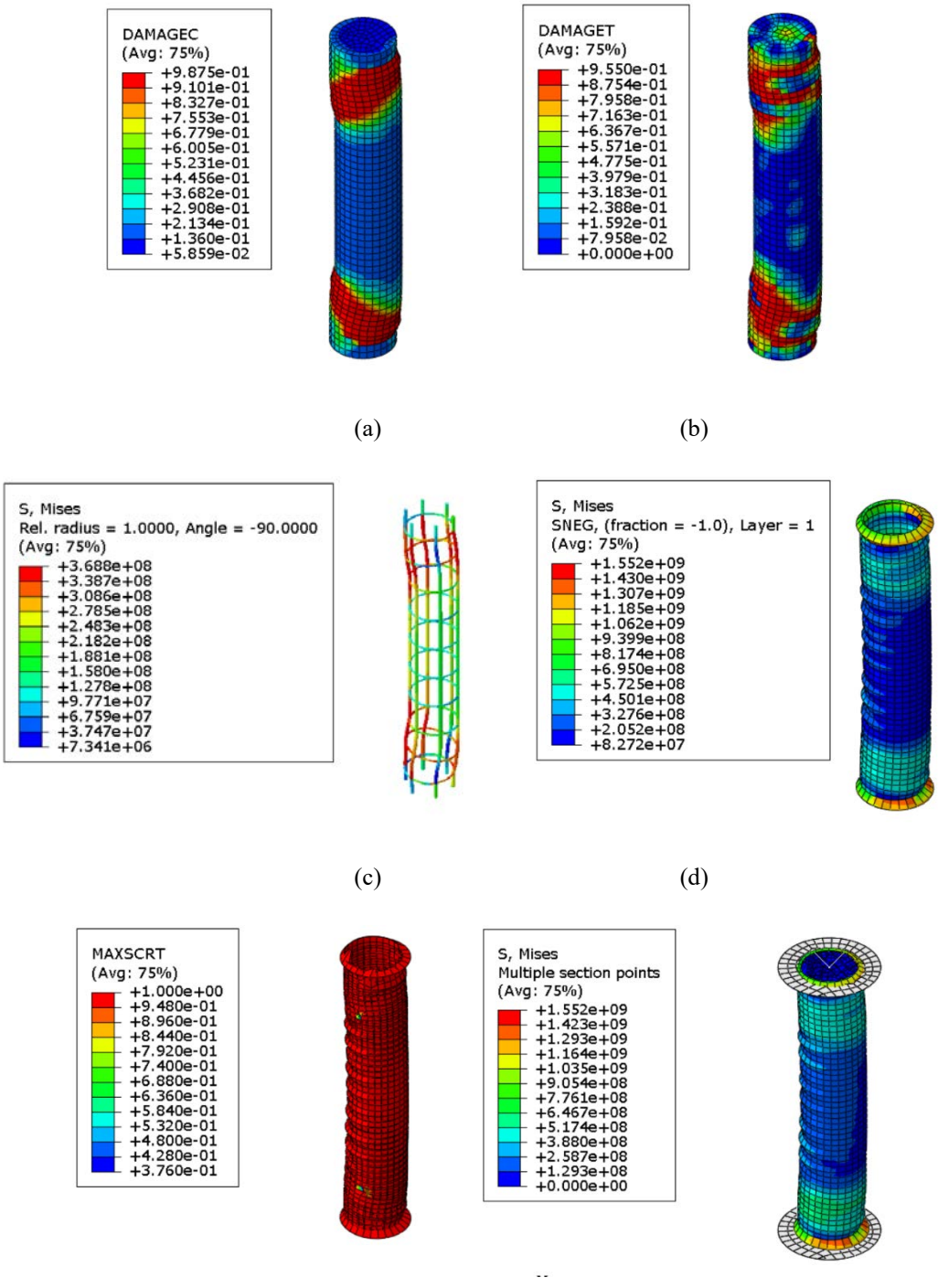

Figure 39: Field Output: Stresses and damage contour in elements (a) Concrete Compressive Damage (b) Concrete Tensile Damage (c) Steel Reinforcement Stresses (d) FRP Stresses (e) Matrix Damage (f) Assembly Stresses

Chapter 6. Conclusion

Finite Element models simulating the behavior of corrosion damaged RC columns were developed. Short and slender columns were subjected to displacement controlled concentric and eccentric loading, respectively. The effect of strengthening with 1, 2, 3 and 4 PBO-FRCM layers are investigated, and the following conclusions are drawn:

1. Confining pre-damaged RC columns with PBO-FRCM layers restored the original axial capacity and enhanced the axial ductility of RC columns at all pre-damage levels for both concentric and eccentric columns.
2. Enhancement in axial capacity and ductility was more pronounced in the circular columns than in the square columns. This is consistent with findings in published literature.
3. Control columns failed by concrete crushing while strengthened columns failed by matrix damage. This is an indication of the effectiveness of the strengthening system irrespective of the cross-section type. This finding is consistent with published experimental study.
4. The load–deformation relationships in all specimen groups are similar when varying the number of PBO-FRCM layers however changing the column cross-section induced a sudden failure mode for the square columns resulting from stress concentration in FRCM.
5. A strong correlation was observed in axial capacity and ductility enhancement with increase in FRCM layers (1, 2, 3 and 4 layers) in concentric columns, consistent with findings in published literature.
6. Increasing the number of FRCM layers also enhanced the axial capacity of eccentrically loaded columns irrespective of damage level and eccentricity ratio, however the axial capacity enhancement diminishes as the damage level and eccentricity get severe. This is consistent with published experimental findings.
7. Comparison of column axial capacity computed using ACI 549.4R-13 provisions against FEA revealed that the code provisions underestimate the axial capacity of short concentric RC columns retrofitted with PBO-FRCM.

8. Using ABQUS to model pre-damaged RC columns retrofitted with PBO-FRCM is effective in accurately predicting the axial capacity and overall behaviour.
9. Three major sources of non-convergence in the finite element model were resolved:
    a. Material nonlinearity was resolved by making the tensile damage in concrete linear since a static analysis is conducted in this study. However, non-linear tensile damage needs to be accounted for in dynamic analysis.
    b. Assembly nonlinearity in the interface between cohesive elements of the matrix, FRP and the concrete surface was resolved by introducing tie constraints between the surfaces. The tie constraints ensure continuity in the analysis in the event of wrinkling of the PBO-FRCM, especially in the eccentrically loaded columns.
    c. Analysis nonlinearity was resolved by using infinitesimal time and step increment and increasing the cutback trial to 50 instead of the ABAQUS default 5. Increasing the cutback trial allows the analysis to rerun the same unsuccessful increment up to 50 times. A single step is expected to converge within 15-20 trials and once convergence is not achieved, the step size and/or mesh size is decreased. A combination of these two tricks was used to improve the analysis convergence.

References

[1] H. M. Shalaby and O. K. Daoud, “Case studies of deterioration of coastal concrete structures in two oil refineries in the Arabian Gulf region,” *Cem. Concr. Res.*, vol. 20, no. 6, pp. 975–985, Nov. 1990.

[2] M. Khanzadeh Moradllo, M. Shekarchi, and M. Hoseini, “Time-dependent performance of concrete surface coatings in tidal zone of marine environment,” *Constr. Build. Mater.*, vol. 30, pp. 198–205, May 2012.

[3] Y.-C. Ou and N. D. Nguyen, “Influences of location of reinforcement corrosion on seismic performance of corroded reinforced concrete beams,” *Eng. Struct.*, vol. 126, pp. 210–223, Nov. 2016.

[4] R. Al-Hammoud, K. Soudki, and T. H. Topper, “Fatigue flexural behavior of corroded reinforced concrete beams repaired with CFRP sheets,” *J. Compos. Constr.*, vol. 15, no. 1, pp. 42–51, 2011.

[5] T. El Maaddawy, K. Soudki, and T. Topper, “Performance evaluation of carbon fiber-reinforced polymer-repaired beams under corrosive environmental conditions,” *ACI Struct. J.*, vol. 104, no. 1, pp. 3–11, 2007.

[6] L. A. Bisby, M. F. Green, and V. K. R. Kodur, “Response to fire of concrete structures that incorporate FRP,” *Prog. Struct. Eng. Mater.*, vol. 7, no. 3, pp. 136–149, 2005.

[7] W. D. Thanasis Triantafillou, Stijn Matthys (UGent) , Katrien Audenaert (UGent) , György Balázs, Michael Blaschko, Hendrik Blontrock, Christoph Czaderski, Emmanuelle David, Angello Di Tomasso, *Bulletin FIB: Externally bonded FRP reinforcement for RC structures*, 14th ed. Lausanne, Switzerland: International Federation for Structural Concrete (fib), pp. 1-130, 2001.

[8] J. C. P. H. Gamage, R. Al-Mahaidi, and M. B. Wong, “Bond characteristics of CFRP plated concrete members under elevated temperatures,” *Compos. Struct.*, vol. 75, no. 1–4, pp. 199–205, Sep. 2006.

[9] M. N. Su, L. Wei, J. H. Zhu, T. Ueda, G. P. Guo, and F. Xing, “Combined Impressed Current Cathodic Protection and FRCM Strengthening for Corrosion-Prone Concrete Structures,” *J. Compos. Constr.*, vol. 23, no. 4, pp. 1–11, 2019.

[10] M. Elghazy, A. El Refai, U. Ebead, and A. Nanni, “Experimental results and modelling of corrosion-damaged concrete beams strengthened with externally-bonded composites,” *Eng. Struct.*, vol. 172, no. June, pp. 172–186, 2018.

[11] M. Elghazy, A. El Refai, U. Ebead, and A. Nanni, “Corrosion-Damaged RC Beams Repaired with Fabric-Reinforced Cementitious Matrix,” *J. Compos. Constr.*, vol. 22, no. 5, pp. 1–13, 2018.

[12] M. Elghazy, A. El Refai, U. A. Ebead, and A. Nanni, “Performance of corrosion-aged Reinforced Concrete (RC) beams rehabilitated with Fabric-Reinforced Cementitious Matrix (FRCM),” *Sustain. Constr. Mater. Technol.*, vol. 2016-August, pp. 1–9, 2016.

[13] F. S. Murgo and C. Mazzotti, “Masonry columns strengthened with FRCM system: Numerical and experimental evaluation,” *Constr. Build. Mater.*, vol. 202, pp. 208–222, 2019.

[14] M. Elghazy, A. El Refai, U. Ebead, and A. Nanni, “Post-repair flexural performance of corrosion-damaged beams rehabilitated with fabric-reinforced cementitious matrix (FRCM),” *Constr. Build. Mater.*, vol. 166, pp. 732–744, 2018.

[15] M. Elghazy, A. El Refai, U. Ebead, and A. Nanni, “Effect of corrosion damage on the flexural performance of RC beams strengthened with FRCM composites,” *Compos. Struct.*, vol. 180, pp. 994–1006, 2017.

[16] A. Jabr, A. El-Ragaby, and F. Ghrib, “Effect of the fiber type and axial stiffness of FRCM on the flexural strengthening of RC beams,” *Fibers*, vol. 5, no. 1, pp. 1–22, 2017.

[17] L. H. Sneed, S. Verre, C. Carloni, and L. Ombres, “Flexural behavior of RC beams strengthened with steel-FRCM composite,” *Eng. Struct.*, vol. 127, pp. 686–699, 2016.

[18] V. Pino, H. Akbari Hadad, F. De Caso Y Basalo, A. Nanni, U. Ali Ebead, and A. El Refai, “Performance of FRCM-Strengthened RC Beams Subject to Fatigue,” *J. Bridg. Eng.*, vol. 22, no. 10, pp. 120–131, 2017.

[19] F. Faleschini, J. Gonzalez-Libreros, M. A. Zanini, L. Hofer, L. Sneed, and C. Pellegrino, “Repair of severely-damaged RC exterior beam-column joints with FRP and FRCM composites,” *Compos. Struct.*, vol. 207, no. April 2018, pp. 352–363, 2019.

[20] A. Younis and U. Ebead, “Bond characteristics of different FRCM systems,” *Constr. Build. Mater.*, vol. 175, pp. 610–620, 2018.

[21] F. G. Carozzi and C. Poggi, “Mechanical properties and debonding strength of Fabric Reinforced Cementitious Matrix (FRCM) systems for masonry strengthening,” *Compos. Part B Eng.*, vol. 70, pp. 215–230, 2015.

[22] L. Ombres and S. Verre, “Structural behaviour of fabric reinforced cementitious matrix (FRCM) strengthened concrete columns under eccentric loading,” *Compos. Part B Eng.*, vol. 75, pp. 235–249, 2015.

[23] P. Colajanni, F. De Domenico, A. Recupero, and N. Spinella, “Concrete columns confined with fibre reinforced cementitious mortars: Experimentation and modelling,” *Constr. Build. Mater.*, vol. 52, pp. 375–384, 2014.

[24] R. Parretti and A. Nanni, “Axial testing of concrete columns confined with carbon FRP: effect of fiber orientation,” *Proc. ICCI 2002*, pp. 1–10, 2002.

[25] M. R. Esfahani, F. U. Mashhad, and M. R. Kianoush, “AXIAL COMPRESSIVE STRENGTH OF REINFORCED Ar ch,” *Concrete*, vol. 18, no. 1, pp. 1–11, 2005.

[26] Y. T. Obaidat, “Structural Retrofitting of Concrete Beams Using FRP - Debonding Issues.,” *Thesis (Doctoral in Structural Mechanics) - Departmet of Construction Sciences, Lund University*. Thesis (Doctoral in Structural Mechanics) - Departmet of Construction Sciences, Lund University, p. 185, 2011.

[27] ACI Committee 549.4R-13, *Guide to Design and Construction of Externally Bonded Fabric-Reinforced Cementitous Matrix (FRCM) Systems for Repair and Strengthening Concrete Structures (ACI 549.4R-13)*, 2013th ed. American Concrete Institute, 2013.

[28] N. Yazdani, E. Beneberu, and A. H. Mohiuddin, “CFRP retrofit of concrete circular columns: Evaluation of design guidelines,” *Compos. Struct.*, vol. 202, no. March, pp. 458–464, 2018.

[29] K. & S. I. Pawtucket (America): Hibbitt, “ABAQUS standard user’s manual. Version 6.11,” vol. IV, 2014.

[30] R. Abokwiek, J. A. Abdalla, R. A. Hawileh, and T. El Maaddawy, “RC Columns Strengthened with NSM-CFRP Strips and CFRP Wraps under Axial and Uniaxial Bending: Experimental Investigation and Capacity Models,” *J. Compos. Constr.*, vol. 25, no. 2, p. 04021009, 2021.

[31] N. Tello, Y. Alhoubi, F. Abed, A. El Refai, and T. El-Maaddawy, “Circular and square columns strengthened with FRCM under concentric load,” *Compos. Struct.*, vol. 255, no. September 2020, p. 113000, 2021.

[32] M. M. A. Kadhim, M. J. Altaee, A. H. Adheem, and A. R. Jawdhari, “A robust 3D finite element model for concrete columns confined by FRCM system,” *MATEC Web Conf.*, vol. 281, p. 01006, 2019.

[33] F. Abed, C. Oucif, Y. Awera, H. H. Mhanna, and H. Alkhraisha, “FE modeling of concrete beams and columns reinforced with FRP composites,” *Def. Technol.*, vol. 17, no. 1, pp. 1–14, 2020.

[34] ACI Commitee 318, *Building Code Requirements for Structural Concrete (ACI 318S-14) and Commentary (ACI 318SR-14)*, 2014th ed. American Concrete Institute, 2014.

Vita

Muhammad Kyaure was born and raised in Nigeria where he received primary and secondary education. In 2013, he moved to Sharjah, United Arab Emirates for the sole purpose of education and he received his B.Sc. degree in Civil Engineering from the American University of Sharjah in 2018. In 2019 he returned to AUS to pursue a master's degree in Civil Engineering with concentration in Structural Engineering while working fulltime.

Professionally, he gained engineering experience working for major contracting companies in the UAE and research experience working as a graduate research assistant in the Department of Civil Engineering at AUS. He met with success when his research on sustainable asphalt in the UAE won first place of Sharjah Sustainability Award 2017. His most recent research on Finite Element Investigation of short RC columns was published by IEEE in 2020.